UNIVERSITÀ DEGLI STUDI DI PADOVA

UNIVERSITA' DEGLI STUDI DI PADOVA

Dipartimento di Ingegneria Industriale DII

Corso di Laurea Magistrale in Ingegneria Energetica

Experimental and theoretical investigations on solar heating and ground source heat pump systems

Relatore: Prof. Anna Stoppato

Correlatore: Prof. Elsabet Nielsen

Prof. Simon Furbo

Studente: Edoardo Callegari

Matricola: 2021386

Anno Accademico 2022/2023

Preface

This thesis was carried out in the Department of Civil Engineering, at the Technical University of Denmark (DTU) in Copenhagen under the supervision of Anna Stoppato, Elsabet Nomonde Noma Nielsen and Simon Furbo, during the Erasmus exchange program between the University of Padua and DTU from January until July 2022.

It is assumed that the reader has a basic knowledge of thermodynamics and heat transfer in order to better understand the main topics covered and the main results.

Riassunto

Poiché uno dei principali obiettivi di questo decennio è quello di limitare il riscaldamento globale e tutte le emissioni legate alle attività umane, la generazione di energia attraverso fonti energetiche rinnovabili (FER) gioca un ruolo cruciale nella creazione di un futuro sostenibile. Riguardo la produzione di acqua calda sanitaria (ACS) e il riscaldamento degli ambienti nel settore residenziale, lo sviluppo di pompe di calore combinate con collettori solari può chiaramente contribuire alla generazione di energia pulita, portando a minori emissioni e riducendo così l'impatto sull'ambiente.

Lo scopo di questa tesi è l'analisi delle proprietà del fluido e delle condizioni di funzionamento tipiche in diversi periodi dell'anno della pompa di calore a sonde geotermiche orizzontali combinata con collettori solari situata presso il dipartimento di Ingegneria civile e meccanica del DTU. Inoltre, è svolta un'indagine sperimentale sullo scambio di calore tra il terreno e la sonda geotermica, utilizzando un campione di suolo. Diversi parametri, come l'*heat exchange capacity rate* (HECR) e la resistenza di contatto tra tubo e suolo, *"pipe soil contact resistance (PSCR)"*, sono stati analizzati con diversi esperimenti al fine di ottenere una comprensione più approfondita dello scambio di calore in diverse condizioni operative. Dall'analisi sul campione di suolo si nota che il trasferimento di calore è principalmente influenzato dal livello di temperatura considerato, dalla temperatura iniziale del suolo e dalla temperatura di ingresso dell'acqua nella sonda, e si verifica meglio in modalità di carica del suolo, "*charging mode"*, che in modalità di scarico del terreno. *"discharging mode"*. I risultati ottenuti per la carica del suolo sono: $HECR_{charging}$ varia tra 5.3 W/K e 6.3 W/K, mentre $PSCR_{C,average} = 0.007$ m^2K/W.

Per quanto riguarda la pompa di calore a sonde geotermiche orizzontali combinata con collettori solari, l'analisi fatta mostra che la densità e il calore specifico del fluido nella sonda sono funzione della temperatura a cui avviene lo scambio termico tra suolo e terreno. Equazioni che descrivono la dipendenza dalla temperatura sono state ricavate. Inoltre, la modalità di "*charging mode"* è stata studiata e confrontata con la modalità di *"discharging mode"*, considerando le ore mensili e i flussi termici. Luglio è il mese con il maggior numero di ore mensili di carica del suolo (299 h), mentre gennaio è il mese con il maggior numero di ore mensili di scarica del suolo (295 h).

Un modello del sistema pompa di calore/collettori solari è realizzato con il software TRNSYS e diversi parametri, come la *"PSCR"* e le proprietà del fluido, sono implementati tenendo conto dei risultati sulle analisi fatte e delle indagini sperimentali sul campione di suolo. L'equazione di Kusuda viene utilizzata per calcolare parametri importanti per i profili iniziali di temperatura del suolo per le simulazioni effettuate. La differenza di temperatura tra l'ingresso e l'uscita della sonda geotermica viene calcolata considerando i valori misurati e calcolati dal modello. I risultati mostrano che la

differenza di temperatura media tra valori misurati e calcolati differisce di 1K per entrambe le simulazioni effettuate.

.

Abstract

As one of the main goals of this decade is to limit global warming and all emissions related to human activities, the generation of energy through renewable energy sources (RES) plays a crucial role in creating a sustainable future. Regarding the production of domestic hot water (DHW) and space heating (SH) in the residential sector, the development of heat pumps combined with solar collectors can clearly contribute in the generation of clean energy, leading to lower emissions and thus reducing the impact on the environment.

The aim of this thesis is an analysis of the fluid properties and of the typical operation conditions in different periods of the year of the horizontal ground source heat pump (HGSHP) combined with solar collectors located at the test facility of the department of civil and mechanical engineering of DTU. An experimental investigation of the heat transfer between soil and ground loop heat exchanger is also carried out by using a soil sample box. Different parameters such as the heat exchange capacity rate (HECR) and the pipe soil contact resistance (PSCR) are investigated in order to gain deeper understanding of the heat exchange with different operating conditions. The measurement box analysis shows that the heat transfer is mainly affected by the temperature level of operation, by the initial soil temperature and by the inlet temperature of the water in the loop, and that it better occurs in charging operating mode than in soil discharging mode. $HECR_{charging}$ varies between 5.3 W/K and 6.3 W/K, while $PSCR_{charging,average} = 0.007$ m^2K/W.

Regarding the GSHP combined with solar collectors, the analysis shows that the density and the specific heat of the fluid in the ground loop are function of the temperature at which the heat transfer between soil and ground occurs. Equations that describe the temperature dependence are obtained. Moreover, the charging operating mode is studied and compared with the discharging operating mode of the GSHP by considering the monthly hours and the energy flows. July is the month with the highest number of charging monthly hours (299 h), while January is the month with the highest number of discharging monthly hours (295 h).

A model of the HGSHE is developed on Transient System Simulation Tool (TRNSYS) software and different parameters, such as the PSCR and the fluid properties, are implemented by taking into account the results from the analysis of the HGSHE and from the experimental investigation of the soil box. The Kusuda equation is used to calculate important parameters for the starting temperature profiles of the soil for the simulations performed. The temperature difference between inlet and outlet of the GSHE is analysed by considering the measured and calculated values from the model. Results show that the average temperature difference between measured and calculated values differs for less than 1K for both simulations performed.

Acknowledgements

First of all, I would like to thank Professor Anna Stoppato for transmitting me her passion for engineering, for her support and encouragement during all the project and for giving me the opportunity to live this incredible experience at DTU university.

I would also like to thank Elsabet Nielsen and Simon Furbo for their supervision in all these months. They encouraged me during all the project with their help. Their wide knowledge helped me to better deal with the investigations I carried out in my thesis.

Moreover, I would like to thank my mum, dad and sister for their support during all these months in Denmark: I am grateful to all of them for encouraging me in this amazing experience I lived and to always believe in me. I also want to thank my friend Anita for all the information she gave me, Emily, Sergio, Daniele, Andrea, Giacomo, Chiara and Rosario for their advices.

Table of Contents

List of Figures

List of Tables

Nomenclature

Symbols

$T_{ambient}$	ambient temperature [°C]
T_{soil}	soil temperature [°C]
T_{in}	water inlet temperature [°C]
T_{out}	water outlet temperature [°C]
m	mass flow rate [kg/s]
c_p	specific heat capacity [kJ/kgK]
ρ	density [kg/m^3]
P	power [W]
m_v	volumetric flow rate [m^3/s]
V	volume [m^3]
$T_{i,average}$	average initial temperature [°C]
$T_{o,average}$	average final temperature [°C]
ΔQ_{soil}	soil energy content variation [Wh]
ΔQ_{water}	water energy content variation [Wh]
ΔQ_{losses}	energy losses [Wh]
ΔT	temperature difference [K]
Δt	time interval [s]
$d_{rockwool}$	rockwool insulation [cm]
S	shape factor
A	surface area [m^2]
HECR	heat exchange capacity rate [W/K]
H	overall heat transfer coefficient [W/m^{2}K]
HTC	heat transfer coefficient [W/m^{2}K]
PSCR	pipe soil contact resistance [m^{2}K/W]
$h_{c,i}$	inner heat transfer coefficient [W/m^{2}K]
$h_{c,o}$	outer heat transfer coefficient [W/m^{2}K]
Nu	Nusselt number
Pr	Prandtl number
Re	Reynolds number

r_i	inner radius [m]
r_y	outer radius [m]
Q_{cM}	heat at the condenser measured [kWh]
Q_{eM}	heat at the evaporator measured [kWh]
Q_{cC}	heat at the condenser calculated [kWh]
P_{eM}	electric power absorbed [kWh]
L	pipe length [m]
λ	thermal conductivity [W/mK]
v_s	kinematic viscosity [m^2/s]

Abbreviations

HGSHE	horizontal ground source heat exchanger
GHG	green house gasses
RES	renewable energy sources
SH	space heating
DHW	domestic hot water
GSHP	ground source heat pump
IPA	isopropyl alcohol
GHI	ground horizontal irradiation [kWh/m^2]
COP	coefficient of performance
SPF	seasonal performance factor
GLHE	ground loop heat exchanger
GSHE	ground source heat exchanger
PID	proportional integrative derivative
SAGSHP	solar assisted ground source heat pump
TRNSYS	transient system simulation tool

1 Introduction

As decades of research and evidence has shown, renewable energy technologies are the key element towards a global transition to a cleaner and more sustainable world. Taking into account that global population growth is leading to greater energy demands and that high levels of fossil fuel consumption still prevent states from reaching the international agreements for Net Zero emissions, a rapid change and restructuring of the energy sector is needed.

Climate change is known to be a big threat for the future and multiple sectors must reduce rapidly their impact to reduce global greenhouse gasses (*GHG*) emissions [1].

Electricity consumption demand is constantly increasing and the residential sector clearly represents a big part of it (Figure 1). It is important that renewable energy sources increase their contribution for the production of heat and electricity in the upcoming years in order to reduce the use of fossil fuels and the related emissions. Figure 1 shows the electricity consumption by sector from 1990 until 2019. The industry sector and the residential sector have the highest share.

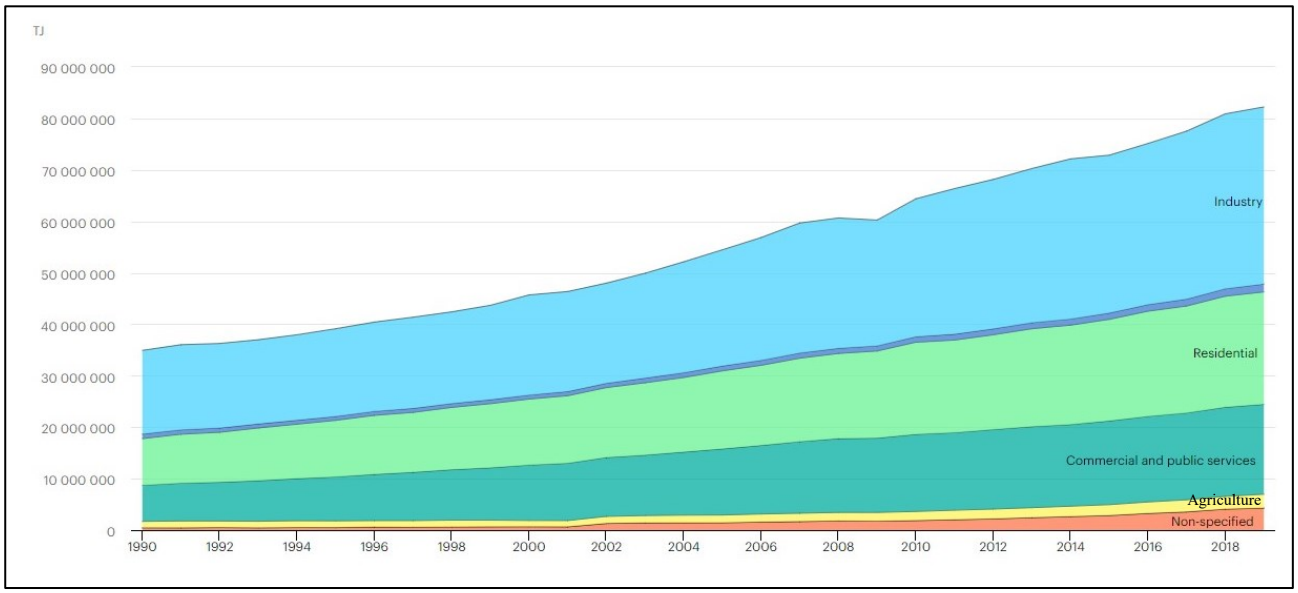

Figure 1: Electricity consumption by sector in the world, 1990 – 2019. [2]

Human activities continuously cause high *GHG* emissions from different sectors such as transport and energy production.

Solar energy, hydro energy and wind energy are clearly promising solutions for the production of electricity and their contribution is expected to increase in the following decades in order to meet the growing energy demand.

Figure 2 shows the renewable electricity generation by source in the world, between 1990 and 2019.

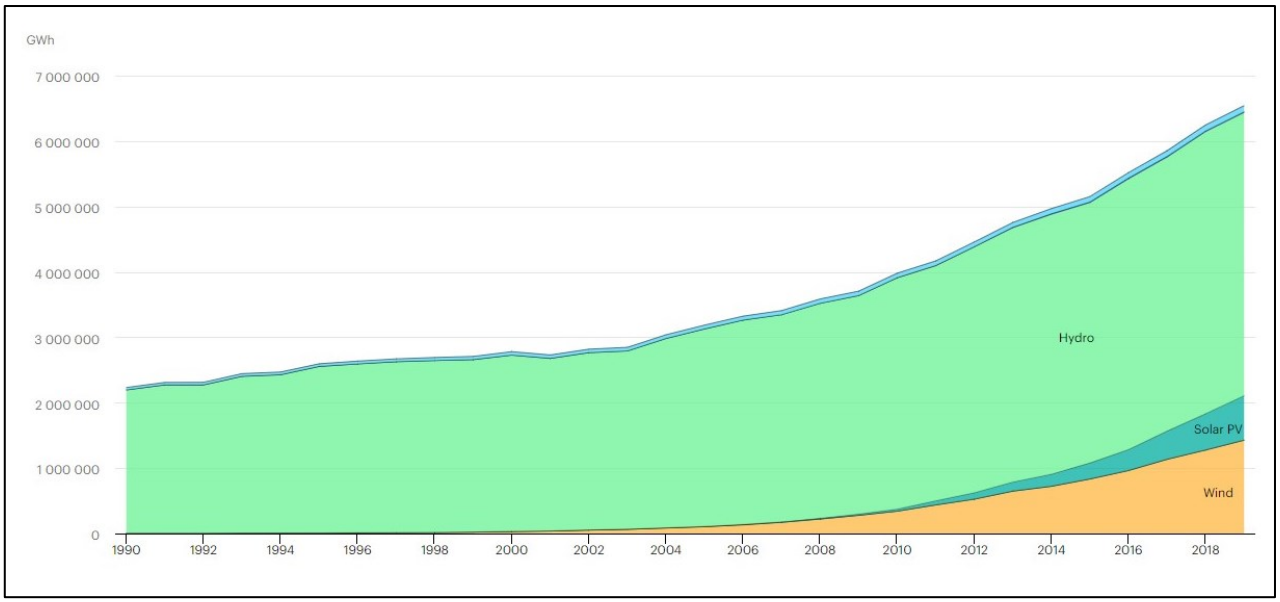

Figure 2: Renewable electricity generation by source in the world between 1990 and 2019. [3]

The total energy consumption is nowadays required mostly for transport, industries and residential activities. In particular, space heating (SH) and domestic hot water (DHW) have the highest energy share concerning the residential sector, precisely 63.6% and 14.8% (Figure 3); the use of RES can lead to a remarkable reduction of the emissions and energy required. The sectors where an active action is needed to reduce the impact on the environment are multiple and focusing on the residential one surely could lead to significant and positive improvements.

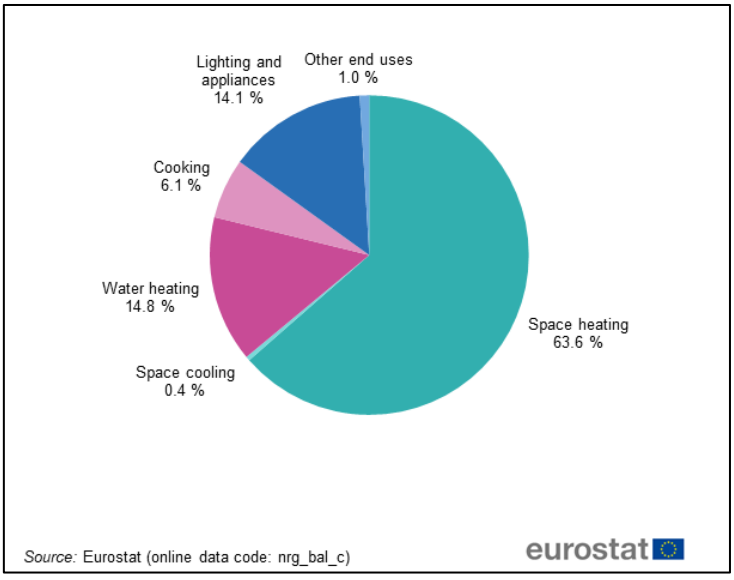

Figure 3: Final energy consumption in the residential sector by use, EU 2019. [4]

Various options of RES for energy systems are possible and new sustainable technologies such as solar collectors and heat pumps are already available on the market and their use can contribute to reduce the environmental impact of thermal system for residential applications. Engineering studies

and knowledge regarding energy production can show which is the best solution to adopt in every situation in order to exploit at the maximum the RES available in a specific location.

1.1 Aim and structure of the project

This master thesis aims to analyse the typical operation conditions in different periods of the year of a ground source heat pump (GSHP) combined with solar collectors located at the DTU campus and to study the heat exchange between the soil and the ground loop heat exchanger by using data collected in 2019.

In chapter 2 some references regarding the operation of heat pumps, the state of the art of ground source heat pumps and the combination with solar collectors are presented.

In chapter 3 data from the analysis of the ground source heat pump operation are used as input for experimental investigations regarding a soil sample that is studied in the laboratory of the DTU civil and mechanical engineering department. The experiments are used to study the heat exchange between the heat transfer fluid and the soil and to get information about the heat exchange capacity rate and other parameters with different operating conditions. Heat balances and experiments are carried out with different temperatures of the fluid and of the soil. For the soil sample experiments pure water is used as fluid, while in the real ground loop of the facility a specific mix of water and isopropyl alcohol (IPA) is adopted.

In chapter 4 the facility at DTU campus is described and thermal properties of the mix water - isopropyl alcohol used in the ground source heat exchanger are investigated, such as density and specific heat. Heat balances regarding the heat transfer between soil and fluid are conducted by analysing data given during the operation of the ground source heat pump in the facility in 2019. Also, the charging of the soil operating mode is analysed in order to clearly understand the typical operation of the system in this condition.

In chapter 5, data from the analysis of the ground source heat pump operation, thermal properties of the heat transfer fluid and data from the experimental investigation of the soil sample are used as input for the TRNSYS model (Transient System Simulation Tool) that is designed. Simulations are performed in order to evaluate the model by comparing data given from the facility with the results of the model under different operating conditions.

Lastly, a summary of the main findings from the experimental investigation and from the results of the TRNSYS model simulation, as well as recommendation for further studies are reported in chapter 6.

2 State of the art of solar and ground source heat pump system

Renewable energy sources always had a key role in the energy transition we have been facing in the past years. Solar energy is an important RES used to get heat from the sun in order to provide the energy requirement both for industrial and residential applications (the generation of domestic hot water but also heat for space heating). However, solar radiation is not a constant source of energy and during the year its availability changes significantly. In Figure 4 it is visible how the global horizontal irradiation (GHI) varies along the year in the location of the DTU university campus in Denmark. It is an example of how the GHI shows the highest values during the summer periods and then it decreases significantly during the winter season. The changeable availability of solar irradiation is the reason why systems both with heat pumps and solar collectors can significantly improve the performance for the production of thermal energy due to their operation modes that are able to cover the heating demand in multiple conditions and periods of the year.

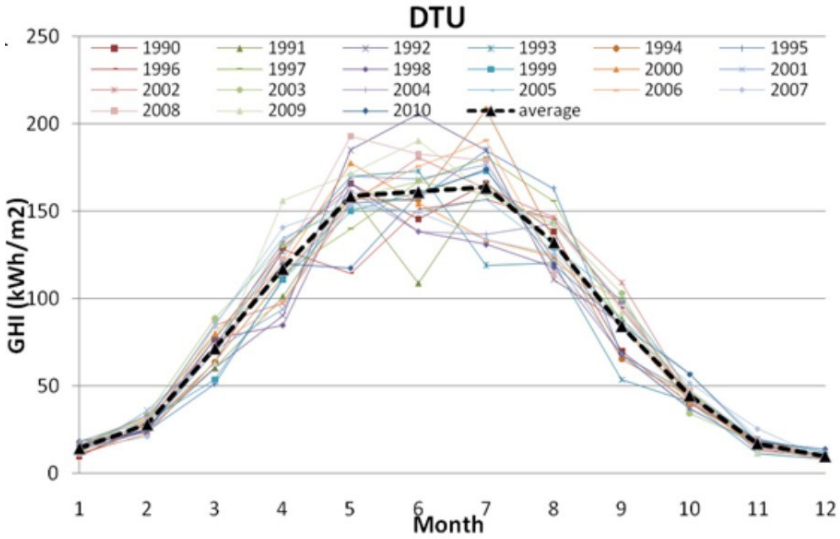

Figure 4: Monthly average GHI [kWh/m^2] at DTU climate station. [5]

A solution to balance the variability of the solar irradiation is the combination of solar collectors with heat pumps. Heat pumps can provide the thermal energy required along the periods of low solar availability and solar collectors instead can provide heat to the users when the solar radiation is available and sufficient. By combining both technologies, it is possible to reduce the electrical energy used by the heat pumps thanks to the contribution of solar collectors and to cover better the heating demand of the users.

Heat pumps absorb electrical energy and can provide thermal energy with considerable high performances compared to other technologies such as gas boiler. Moreover, if the electricity absorbed is generated with RES, the operation of heat pumps is totally clean without any CO_2 emission.

Heat pumps are an important technology that can help to have cleaner source of thermal generation. In the past years the role of heat pumps gained a lot of importance and their share in the thermal generation has increased both in the industrial and residential sector. Almost 180 million heat pumps were used for heating in 2020, as the global stock increased nearly 10% per year over the past 5 years. Heat pumps have become the most common technology in newly built houses in many countries, but still only meet 7% of global building heating demand, yet they could easily supply more than 90% of global space and water heating at a lower CO_2 emissions level [6].

A further increase in the share market of heat pumps for thermal energy production is expected. Currently heat pumps have a share of 9% among the heating technologies sold globally for residential and service buildings. According to the Net Zero Scenario [6], this value is expected to increase up to 30% in 2025 and 42% in 2030. The contribution of heat pumps in the heating generation both for the residential sector and service building is clearly a big challenge but a feasible path to reduce the impact of these sectors.

As proof of the upcoming increase in the heat pump market, is the new decision taken by the government of Netherlands in May 2022 to make heat pumps mandatory from 2026; indeed heating system in Netherlands are covered by fossil gas boiler (71% of the residential heating demand) and citizens have been hit hard by the record gas prices of the past months [7]. Other countries such as Italy, where natural gas has around 60% share of the heat generation, should also take more decisions in the direction of thermal energy systems based on heat pumps [8].

Indeed, pushing to a wider use of heat pumps could lead to lower emissions but also it is a clever solution to reduce the dependence from the volatility of gas prices.

Furthermore, the energy required for space and water heating is foreseen to decrease consistently in the next years and this reduction could be gained by the wide use of heat pumps, which are usually 3 – 4 times more efficient than fossil fuel boilers [2].

2.1 Heat pumps working principle

In the past years, a lot of research has been done concerning technologies for domestic heating with low energy consumption. Heat pumps are suitable solutions to fulfil the thermal energy requirements for residential buildings.

Heat pumps work by extracting heat from one environment (the heat source) and transferring it to another (the heat sink), generally by using a compressor to circulate a refrigerant fluid through a vapour - compression refrigeration cycle. Under favourable conditions, the amount of thermal energy transferred can be significantly higher (three to five times) than the energy used to drive the compressor, resulting in high efficiency for heating devices. This ratio between useful heat

delivered and energy input defines a heat pump's coefficient of performance (COP) and its yearly average value, the seasonal performance factor (SPF), both of which reflect system efficiency. As efficiency decreases significantly when the difference in temperature between the heat sink and the heat source increases, heat pump effectiveness depends on both the climate, the building's insulation and the heat distribution system [9].

Heat pumps are generally made of 4 important elements: evaporator, compressor, condenser and expansion valve.

In the evaporator the refrigerant absorbs heat from the heat source (air, water or ground) and evaporates, then the compressor absorbs electrical energy and increases the pressure and the temperature of the refrigerant. In the condenser the refrigerant condenses and releases heat which is the goal of the operation. Lastly, thanks to the expansion valve the refrigerant goes back to the starting values of pressure and temperature, and the cycle can start again.

Figure 5 shows the general scheme of a heat pump.

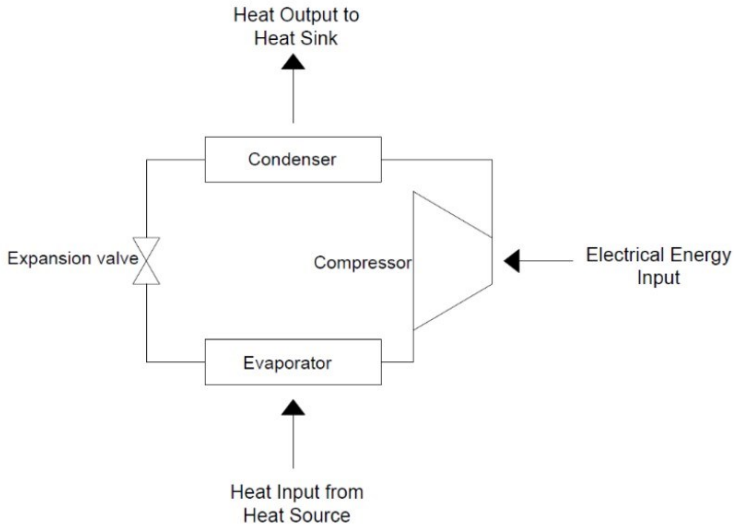

Figure 5: Scheme of heat pump with different components and heat flows.

2.2 Types of heat pumps

There are several types of heat pumps with different heat sources. Indeed, it can be possible to use air, water or ground to absorb heat from the outside environment.

The performance of heat pumps that use air as heat source strongly depends on the external air temperature. The lower is the outside temperature the higher the temperature difference between cold and hot sink, the lower the efficiency (Figure 6).

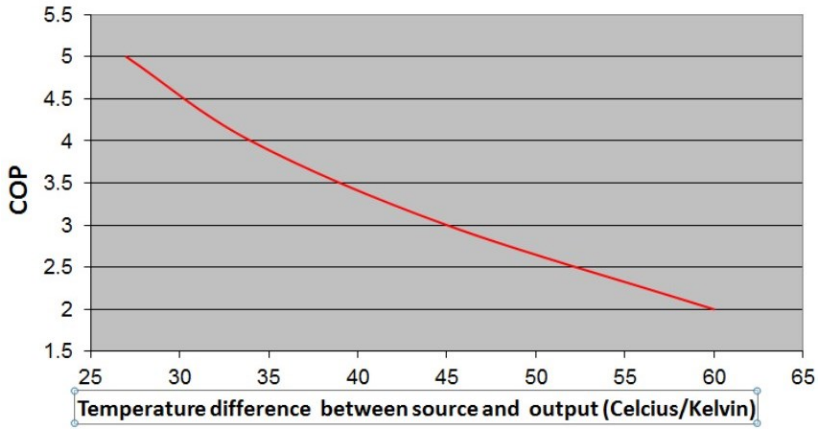

Figure 6: COP Variation depending on temperature difference between hot sink and cold sink. [10]

In countries like Denmark, the temperature of the air varies a lot along the year: a possible configuration for the installation of heat pumps in this location is by using the ground as heat source.

As shown by [11], GSHPs have a lower consumption of electricity compared to air heat pumps because defrosting is not needed and thus some energy can be saved. GSHPs are less common globally but compared to air heat pumps they use a more constant heat source that is the ground; for this reason, the efficiency achieved by GSHPs can be higher with the right configuration and design. The ground temperature is indeed higher than the air temperature on average during the winter and colder than the air in the summer. GSHPs takes advantage of these more favourable temperatures to become highly efficient by exchanging heat with the soil through a ground loop heat exchanger (GLHE). As shown in the study [12], GSHPs are able to gain in specific conditions an average seasonal performance factor of 3.3, while air heat pumps of 2.6: this is due to the more stable and constant temperature of the ground during the year compared to the air temperature. Indeed the ground temperature has a smaller range of variation during different seasons of the year and thus the SPF is less affected compared to air heat pumps.

In Figure 7 heat pumps share by source and other possible arrangements with renewable energy sources are given. Air and ground heat pumps are clearly the most widely used heat pumps technology.

Nevertheless, the installation costs for GSHPs are higher compared to air heat pumps, but the economic aspects are not considered in this thesis.

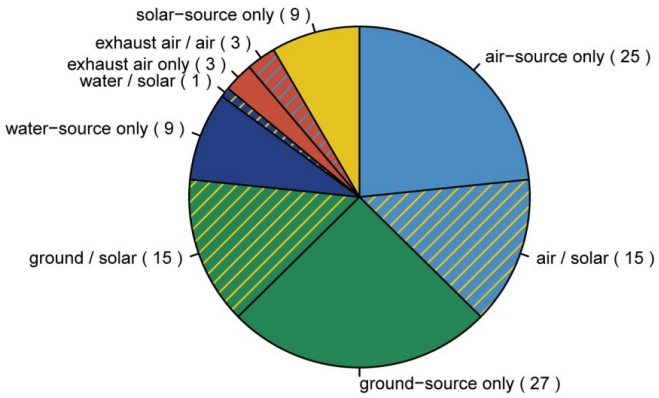

Figure 7: types of heat pumps and more common combinations sold in the global market. [13]

2.3 Ground source heat pumps

GSHPs can use water reservoirs or the ground as source of heat. Figure 8 shows the number of GSHPs in different European countries. Sweden has the highest number thanks to its policy and incentives regarding heating systems but also thanks to its geographic location. Indeed, in this country the use of air heat pumps would lead to lower performances compared to GSHPs due to the higher variability of the air temperature compared to the ground along the year.

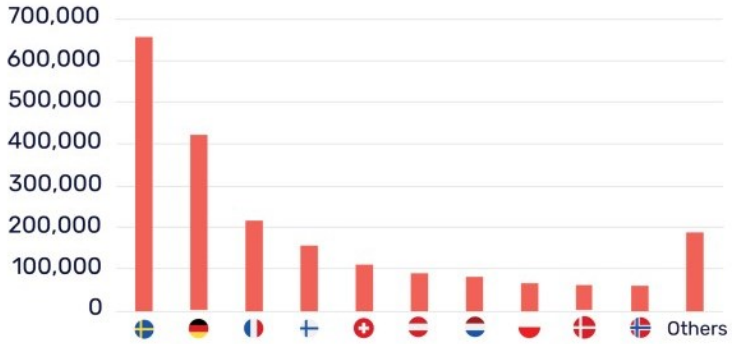

Figure 8: Number of ground source heat pumps in Europe. [14]

There can be two main possible configurations for GCHP: open loop systems or closed loop systems. Several factors such as climate, soil conditions, available land, and local installation costs determine which is the best for a site. In order to guarantee an effective operation of the GSHPs the design of the system is important.

Open loop systems use well or surface body water as the heat exchange fluid that circulates directly through the GSHP system. Once it has circulated through the system, the water returns to the ground through the recharge well or through surface discharge. This option is obviously practical only where there is an adequate supply of relatively clean water, and all local codes and regulations regarding groundwater discharge are met [15].

Closed loop systems circulate an antifreeze solution through a closed loop that is buried in the ground or submerged in water. A heat exchanger, usually a plate heat exchanger, is used to transfer heat between the refrigerant in the heat pump and the antifreeze solution in the closed loop.

There can be two main configurations for closed loop systems: with direct exchange or with secondary loop.

In the direct exchange GSHP, the refrigerant absorbs directly heat from the ground; the disadvantage of this configuration is the high amount of refrigerant required and the larger compressor needed. Moreover, because of the refrigerant circulated through the ground, local environmental regulations may prohibit their use in some locations in order to avoid any risk of leakages.

With a secondary loop instead, water with an anti-freezing liquid exchanges heat in the ground and then goes inside the heat pump and releases heat to the refrigerant in the evaporator.

The ground loop heat exchangers in which the fluid is sent to the ground can have two possible configurations: horizontal or vertical (Figure 9).

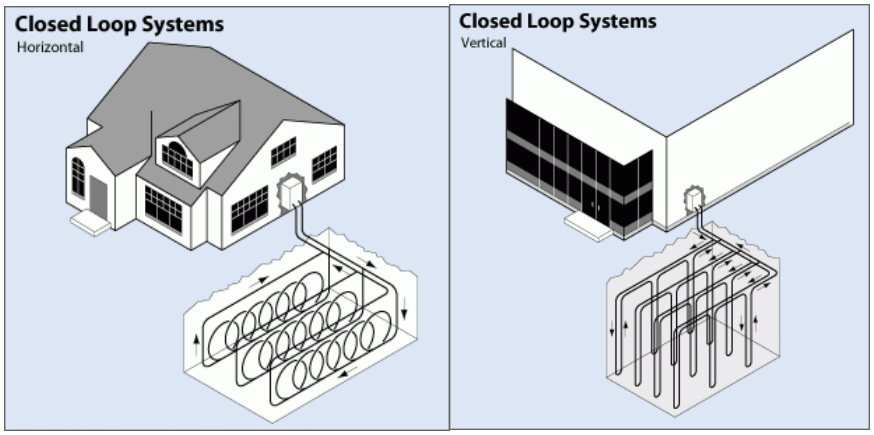

Figure 9: Possible configurations of closed ground loop systems. [16]

The vertical configuration has a lower dependence from the environmental temperature compared to the horizontal one because a deeper depth is reached along the heat exchange (that means more constant temperatures with smaller yearly variation compared to air temperature) and it requires a smaller area, but the costs of installation are higher.

On the other hand, the horizontal ground loop has lower installation cost but a wider area for the installation is required. In this thesis the facility studied at DTU campus has a horizontal ground loop heat exchanger with a mixture of water and isopropyl alcohol in the secondary ground loop. In the following chapters the properties of this secondary ground loop fluid are analysed and discussed.

The focus of this thesis regards the horizontal configuration of GSHP, whose interest has increased in the recent years.

The horizontal configuration no longer requires excessive underground area and it can be applied in multiple locations instead of the vertical configuration, bringing large economic advantages for the installation.

The main parameters of the horizontal heat exchangers are divided into environmental and design. Environmental factors include soil physical properties, meteorological conditions and heating and cooling load, while design factors include the scheme configuration, pipe length, pipe spacing, burial depth, pipe layer, pipe diameter and the fluid flow rate in the ground loop. Current studies showed that the main affecting factors of the system are the design factors. Moreover, by considering the environmental factors in the design process, a decrease in the pipes length up to 60% could be achieved, as shown in [17].

2.4 Integration of solar collectors with ground source heat pumps

The purpose of integrated applications of solar heating system and ground couple heat pumps are to complement each other perfectly and to fully utilize renewable resources for low-carbon and energy saving solutions.

Heat pumps are an excellent low carbon heating solution, but they absorb electricity to run and therefore combining them with solar panels able to contribute to the production of hot water will reduce the electricity needed and the emissions related to the heat pumps operation, as well as cover better the heating demand.

By using a refrigerant cycle, GSHP can export heat from one source (the ground) to another one (the building) in the heating mode, the opposite configuration when cooling the building. They can be used both for heating and cooling demand because of the soil temperature trend along the year. Indeed, during the winter the ground is warmer than the air temperature, while in summer is the opposite and for this reason a double operation of the GSHP for heating and cooling is guaranteed. Moreover, because of the low dependence from the air temperature, high flexibility in different conditions is fulfilled by GSHP.

Solar collectors are able to heat the water (or make the refrigerant evaporates if direct solar assisted heat pump system) and thus the electricity consumption of the heat pump can be reduced leading to an increase of the overall efficiency of the system.

In the last years GSHP combined with solar collectors gained a significant interest due to the high potential in improving residential thermal applications.

The advantages for this configuration are many, such as the higher performances that can be achieved and the wider range of conditions in which combined systems with GSHP and solar collectors can operate. Indeed a full scale heating or cooling operation is achieved in all the seasons: implementing solar energy through solar collectors is a reliable solution, due to the profitable investment costs and maintenance costs but it is dependent on solar radiation, thus it is not enough to cover the heating demand. A combination with GSHP is advantageous in order to provide energy throughout the whole year.
Moreover, the advantage of using a GSHP combined with solar collectors is that the thermal requirements are fulfilled even during night time when the collectors don't operate.
The use of solar panels increases the efficiency of a GSHP, and vice versa, ensuring that the residential users will benefit of this combination. For example, as shown in [18], the coefficient of performance (COP) increases from 3.5 to 4.2 when a GSHP is used combined with solar collectors. Also, other research confirmed this increase of the efficiency with the use of solar collectors but also they showed a reduction of around 70% of the electricity used by the heat pump, leading to economic and environmental advantages [19]. Indeed, solar collectors provide heat to the system and they lead to a decrease in the electricity absorbed by the heat pump in order to fulfil the thermal load.

Coupling a GSHP and solar collectors is clearly a worthwhile solution for several reasons; one more reason is the possibility to send the heat absorbed by the solar collectors to the ground in periods of low heating demand or not sufficient solar radiation to heat up a water storage tank. This way of operating is called charging operating mode and it is another possible way of running the solar collectors and GSHP system. Solar collectors are connected both to a storage tank but also to the ground loop and when there is excess of heat for example during summer days or when the temperature of the solar collector fluid is not high enough to be stored in a tank, the solar collectors send the heated water to the ground. The ground loop releases heat to the soil and by doing this the heat stored in the soil can be partially recovered when it is needed by the users. Partially means that of course a part of the thermal energy sent to the soil by the solar collectors is lost due to heat dispersion in the ground. As shown by [20], with the charging operating mode it is possible to increase the efficiency of energy systems based on GSHP and solar collectors by 19%.
In the following pages the charging operating mode is analysed and described in detail for the facility considered.

There are multiple configurations for a system with GSHP and solar collectors. In this thesis the focus is on the parallel solar assisted heat pump system. Figure 10 shows a general scheme of this configuration. Solar collectors and the heat pumps work in parallel.

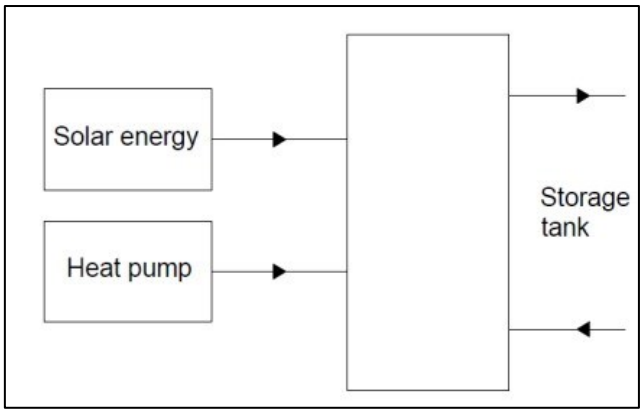

Figure 10: Parallel configuration for the operation of the heat pump and solar energy source. [21]

When the solar collectors are able to produce hot water at the required temperature for the heat storage, they send it to the tank and the GSHP doesn't need to operate. In this configuration sun radiation can be exploited at maximum (Figure 11).

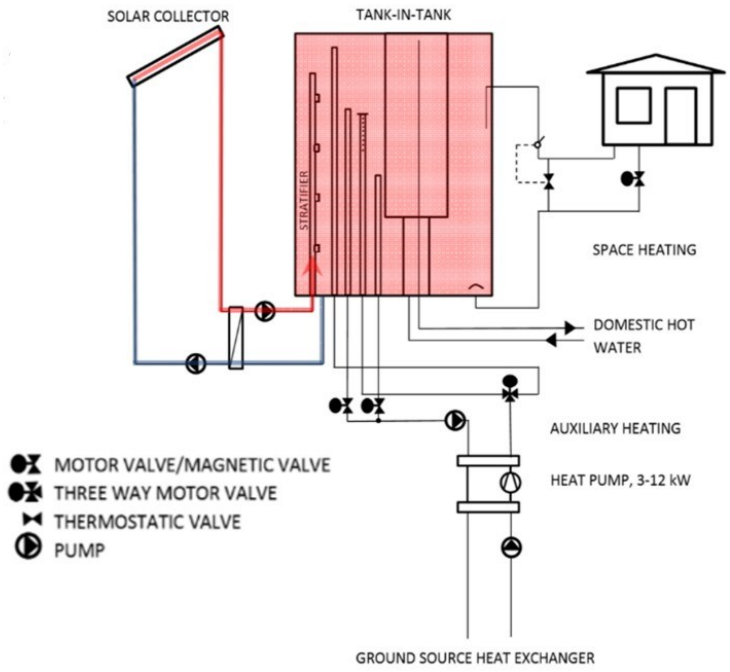

Figure 11: Example of system with GSHP and solar collectors in operation, heat from collectors to the tank. [22]

When instead solar collectors can't meet the heat demand of the heat storage because of low solar radiation or night time, the heat pump starts working and it extracts the required heat from the ground and delivers it to the heat storage. The hot water can be delivered on the top or in a different location in the heat storage depending on the temperature of production, in order to support thermal stratification (Figure 12).

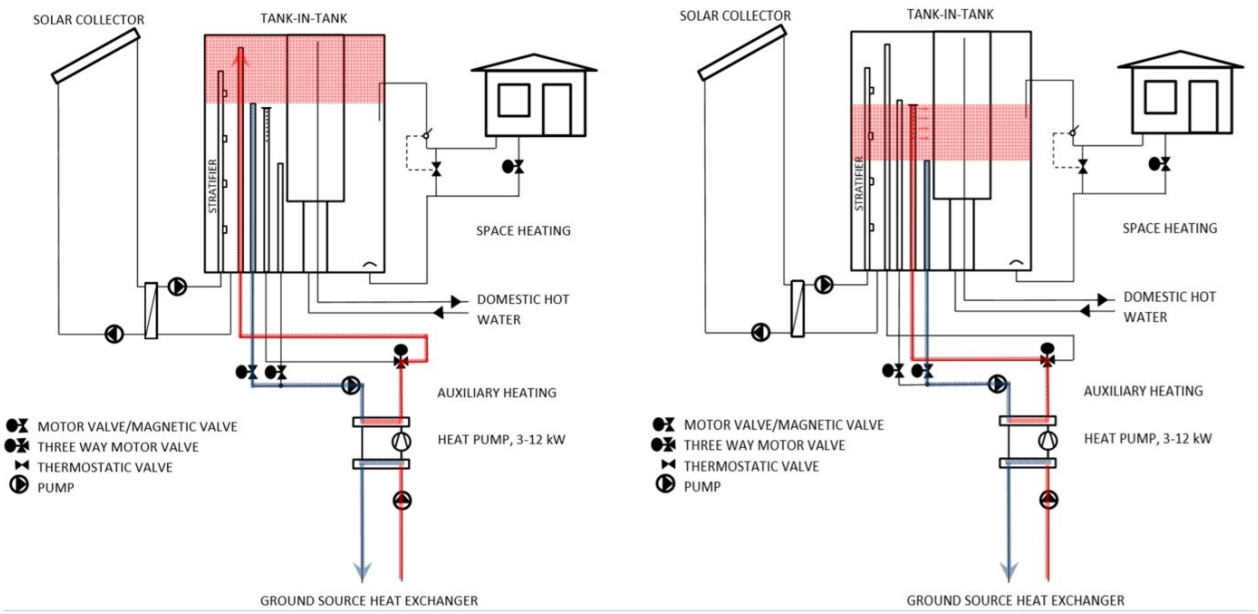

Figure 12: Operation of the GSHP for the production of DHW (on the left) and SH water (on the right). [22]

Moreover, as previously mentioned, the charging operating mode is the third configuration that connects the solar collectors with the ground loop heat exchanger. It has the advantage of sending energy absorbed by the collectors to the ground when it is not needed by the storage tank (Figure 13). This energy increases the soil temperature around the ground loop and consequently part of it is available when the heat pump is in operation, thus when energy is sent from the ground to the storage tank.

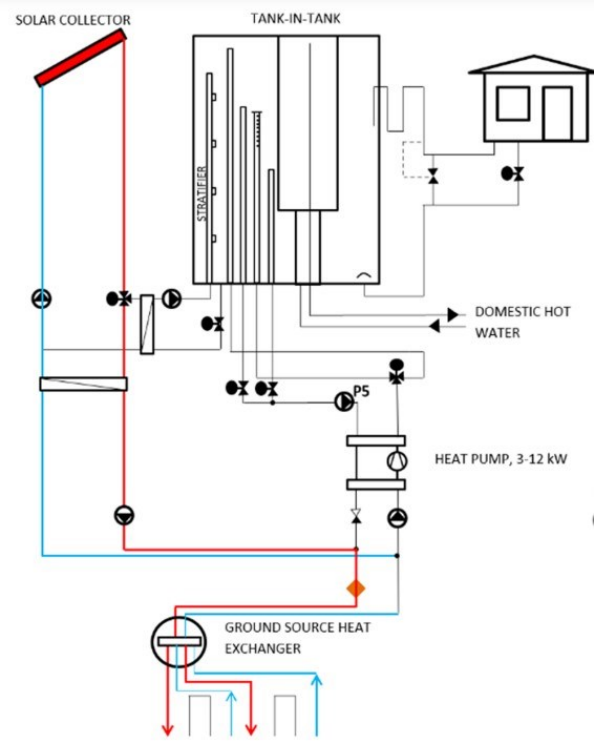

Figure 13: Charging of the soil (regeneration mode). [22]

The heat storage is a tank correctly sized for the thermal users considered. In the parallel configuration it is connected with the solar collectors and the ground loop. Because solar energy has the properties of low energy density and intermittent supply, energy storage tank is a key component to ensure the availability and reliability of heat supply systems. Using a tank to store heat during for example the hours of high radiation, the heap pump also reduces the consumption of electricity because the number of switches on-off is lower compared to a solution without a storage tank. Indeed, the storage leads to a higher average mean temperature because of its thermal inertia.
Both solar collectors and storage tank are key elements to gain a high system performance when a ground source heat pump is in operation [21].

Solar collectors and heat pumps can be used both for DHW production and SH water. DHW requires a higher temperature (typically around 50°C) compared to SH water (typically 35°C). For this reason, with the use of an appropriate storage tank, thermal stratification can be established in the tank. DHW can be stored in the higher part of the tank where warm water rises, while SH water stays in the lower part of the tank.
Thermal stratification of the water inside the tank has performance advantages. The low temperatures at the bottom of the tank ensure a high thermal performance of the solar collectors, and the high temperatures in the top of the tank ensure that the heat is directly usable and the energy supply from the auxiliary energy system, that could be heat pump or gas boiler, is reduced.

It is therefore important that the tank is designed in such a way the thermal stratification under typical operation conditions becomes as large as possible.

3 Experimental investigation on the heat transfer between soil and ground source heat exchanger

This chapter describes the experimental investigation that is carried out in order to study the heat transfer between the soil and the ground source heat exchanger by analysing the variation of the heat exchange capacity rate (HECR) and other parameters with different operating conditions. The soil sample is located in the laboratory of the DTU civil and mechanical engineering department. Set up of the experiments, analysis method and results are shown in the next paragraphs.

3.1 Description of the set up

An insulated soil sample of 1 m^3 with inside gravel and mulch laid in a precise arrangement is used for the investigation. Mulch is placed around the pipe in a 20 cm radius, while the remaining space of the experiment box is filled with gravel. Moreover, a central pipe of 1 m goes inside the soil sample in order to simulate a part of the ground loop heat exchanger. The pipe is made of polyethylene.

Inside half of the soil sample 29 thermocouples for temperature measurements are located in a precise geometry in 3 different semi circles, while 2 sensors are in the corners. The reason why sensors are located just in half of the measurement box is that a symmetric distribution of the heat exchange and of the temperatures is assumed. Figure 14 shows the section of the soil sample with the temperature sensors.

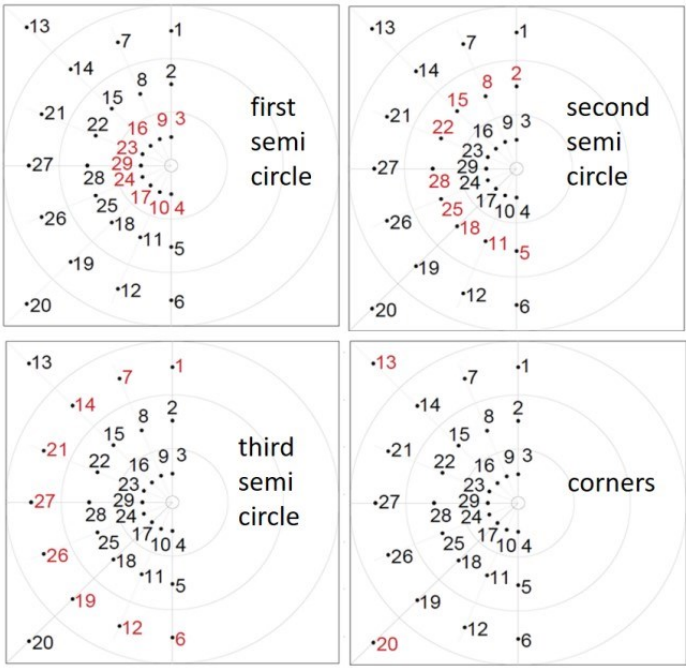

Figure 14: Representation of temperature sensors in the box.

There are also sensors for the inlet and outlet temperature of the water that goes through the central pipe (Figure 15).

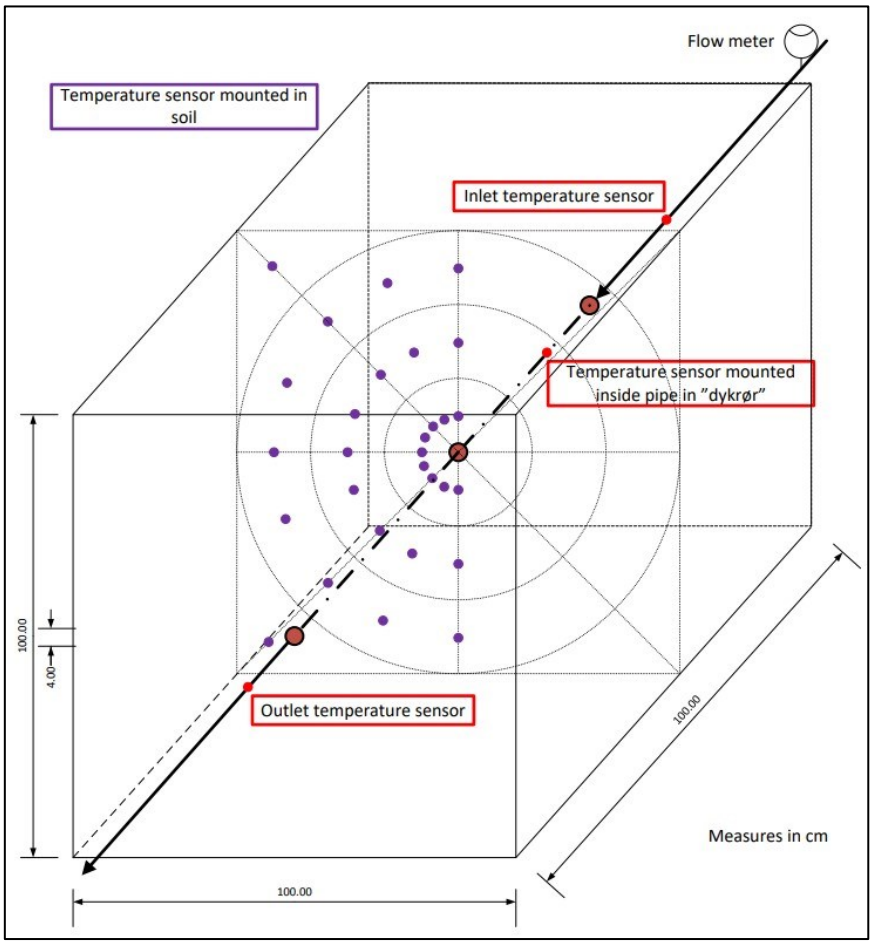

Figure 15:measurement box and location of the soil and water temperature sensors.

Two flowmeters are also positioned to show the mass flow rate in two circuits as shown in Figure 16. Both the thermocouples and the flowmeters have been already calibrated by [23]. It is also visible the 20 cm rockwool of insulation in order to minimize thermal losses with the external ambient.

Along the year the temperature of the ground varies significantly, and for this reason the measurement soil box is connected to a circuit for cooling and heating power supply in order to change the operation conditions of the experiments by simulating different seasonal temperatures of the soil and of the water. Two radiators are placed on the top and bottom of the box for the cooling down or heating up of the soil.

Thanks to multiple valves it is possible to swich from the cooling mode to the heating one. The cooling system uses the cooling circuit of the university, while an electric boiler is used to heat the water for the heating operation mode. It is possible to send cool or warm water just in the central pipe or also in the radiators to modify the operating condition of the experiments.

A bypass can be also used by adjusting in the proper position the valves at the inlet of the inner tube in order to avoid sending water inside the box before it has the desired constant temperature. It is important to check the position of the valves at the start of each experiment in order to achieve the desired flowrate (Figure 16).

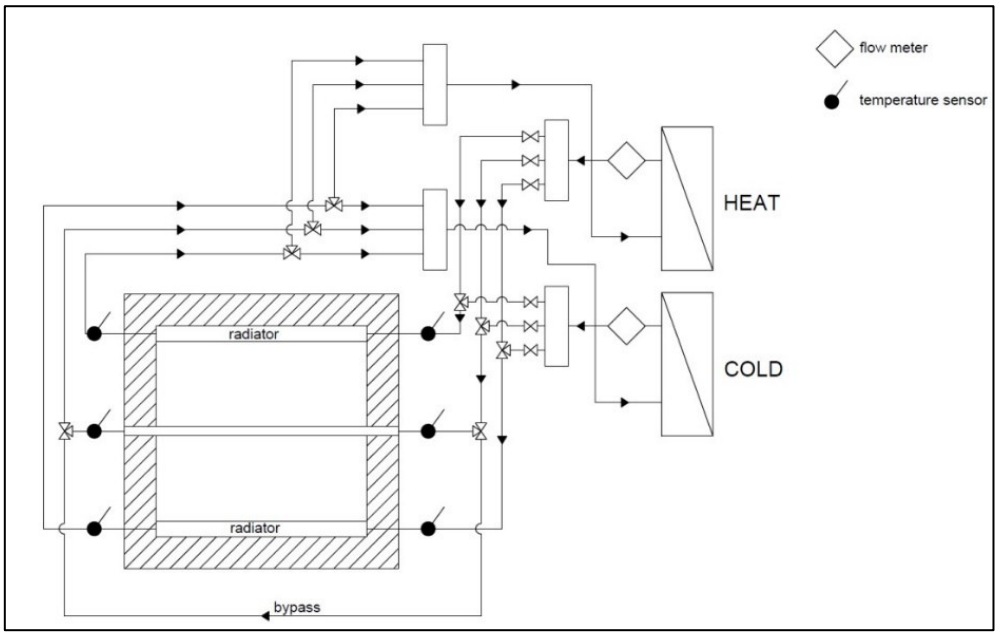

Figure 16: Schematic set up of the connections between the soil box and the cooling – heating systems.

Regarding the cooling mode, it is possible to choose a fixed temperature at which the water or the soil is cooled down. The cooling power is regulated by an automatic throttle valve. An output of 0 – 5 V is sent from a PID controller to the actuator of the throttle valve in order to adapt the throttle proportionally to the voltage, by taking in consideration the set temperature.
Regarding the heating mode, it is possible to set a specific temperature of the water in the boiler to send in the inner tube of the soil box. The power of the electric boiler can vary from 3 kW to 27 kW. When operating with the heating circuit by using the electric boiler, the configuration is the charging one, which simulate the operation of sending heated water from the solar collectors to the soil.

The electric boiler, the throttle valve and the soil box are shown in Figure 17.

Figure 17: Coolant valve (top left), electric boiler (top right), soil box with insulation and pipes (bottom).

The two circuits for cooling and heating are used by opening in the correct way the three way valves. Both circuits are divided by heat exchangers from the loop that goes in the inner pipe and in the two radiators. This loop is indeed closed. The pipes of the system are flexible and connect the heat exchangers, the radiators and the center pipe.

Two manifolds are placed in order to connect the circuits. The left manifold (supply manifold) in Figure 18 has two inlets, one for the cooling supply and the other one for the heating supply. Both inlets have a flowmeter installed for the measurement of the flow rate. There are then three outlets, for the two radiators and the inner pipe of the soil box. The right manifold (return manifold) has instead three inlets, two from the radiators and one from the inner pipe, and two outlets that goes to the cooling or heating heat exchangers. In both manifolds, three way valves are installed and they must be positioned correctly in order to run the experiments without mistakes.

Figure 18 shows the set up and the heat exchanger (bottom left) of the cooling loop with insulation in order to reduce thermal losses. The heat exchanger for the heating loop is located instead close to the electric boiler. Air valves and pressure gauge are places at the top of the manifolds for safety reasons and an expansion vessel is included in the heating operating mode to prevent possible damages in case of water expansion. Two pumps are used, one for the cooling loop and one for the heating loop.

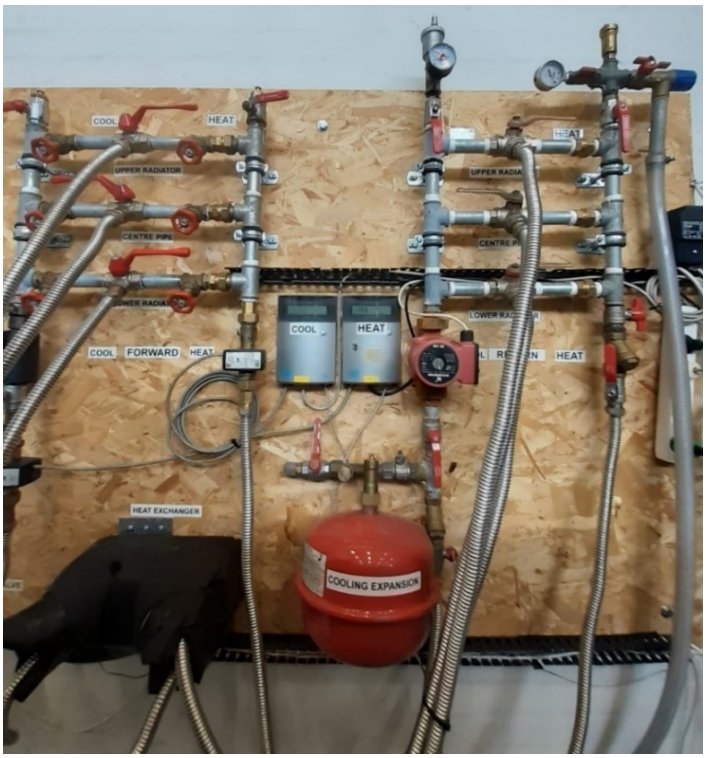

Figure 18: Picture of the set up. Supply manifold on the left, return manifold on the right.

Temperature sensors are connected to the acquisition system in order to analyse the variation of the soil and water temperatures during the experiments, while the water flow rate can be read manually from the flowmeters. Temperature of the soil, inlet – outlet water temperature in the center pipe and in the radiators are monitored. The thermocouples in the pipes are placed in counter flow in order to get precise measurements, and some information can be seen in Figure 19.

Equiment	Name	Location	Accuracy
Temperature sensor	TT type thermocouple copper/constantan	30 pcs in measurement box 6 pcs radiators/PE pipe loop	± 0.1 K
Flow sensor	Brunata HGQ1-R3	1 pc supply cooling loop 1 pc supply heating loop	± 0.5 %

Figure 19: Sensors used for the measurements.

3.2 Analysis method

In this section the parameters taken in consideration for the experiments are explained. During all the measurements, data from the thermocouples are collected with the use of a data logger and printed in an Excel file; values from the flowmeters are read manually and the flow rate is set as low as possible in each experiment in order to have a considerable temperature variation between inlet and outlet in the inner pipe. Figure 20 shows the soil sample and the working desk with the acquisitions system.

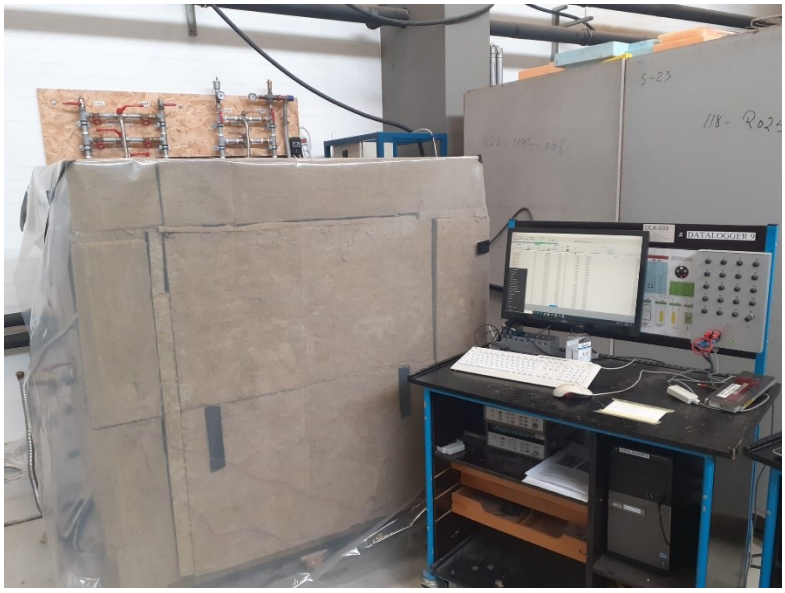

Figure 20: working desk with data acquisition system.

For the analysis method, different parameters are taken in consideration and are explained below.

3.2.1 Heat exchange capacity rate and power exchanged

The heat exchange capacity rate [W/K] is an important parameter during heat transfer phenomena and it gives information regarding the efficiency of the heat exchange between water and soil. It shows how much power is exchanged as funtion of the temperatures of the water and of the soil.
It depends on the temperature of the soil (T_{soil}), inlet and outlet temperature of the water in the inner pipe (T_{in} and T_{out}), the flow rate of the water ($m_{v,water}$), the specific heat of the water ($c_{p,water}$) and the density of water (ρ_{water}). It is given by [23]:

$$HECR = -m_{v,water} * c_{p,water} * \rho_{water} * ln\left(1 - \frac{T_{in}-T_{out}}{T_{in}-T_{mean,soil}}\right) \qquad (3.1)$$

Where $T_{mean,soil}$ is the weighted average of the soil temperatures, determined with equation 3.10, of the three semi-circle in the timestep considered for the data acquisition.
The power [W] exchanged during the experiments is instead calculated by using the volumetric flow rate of the water ($m_{v,water}$), the specific heat of the water ($c_{p,water}$), the density of water (ρ_{water})

and the temperature difference of the water (ΔT_{water}) between outlet and inlet in discharging operating mode or between inlet and outlet in charging operating mode. It is given by:

$$P = m_{v,water} * c_{p_{water}} * \rho_{water} * \Delta T_{water} \quad (3.\ 2)$$

3.2.2 Soil energy content change

The soil volume is conceptually divided in different sections in order to a have a precise calculation of the soil energy content change: 3 circular sections considering the location of the sensors and 1 section considering the remaining part of the soil, basically the corners. The soil energy content change depends on the volume of the part considered (V_{part}), the density of soil (ρ_{soil}), the specific heat of the soil ($c_{v,soil}$), the final and initial average temperature of the soil part considered ($T_{i,average}$ and $T_{0,average}$).

The soil energy content change in the considered part $\Delta Q_{soil,part}$ [Wh] is given by:

$$\Delta Q_{soil,part} = V_{part} * \rho_{soil} * c_{v,soil} * \left(T_{i,average} - T_{0,average}\right) * \frac{1}{3600} \quad (3.\ 3)$$

Where $c_{v,soil}$ is different if it is mulch or gravel (values taken from [23]).

Then the total energy change of the soil $\Delta Q_{soil,tot}$ considering the 4 sections is given by:

$$\Delta Q_{soil,tot} = \Delta Q_{soil,circle1} + \Delta Q_{soil,circle2} + \Delta Q_{soil,circle3} + \Delta Q_{soil,corners} \quad (3.\ 4)$$

3.2.3 Water energy content change

The water releases or absorbs energy from the soil sample. The equation to calculate the energy change in the water while it passes through the soil sample depends on the flow rate of the water ($m_{v,water}$), the specific heat of water ($c_{p,water}$), the density of water (ρ_{water}), the outlet and inlet temperature of the water (T_{out} and T_{in}) and the acquisition time (Δt).

The water energy content variation $\Delta Q_{soil,water}$ [Wh] is given by:

$$\Delta Q_{water} = m_{v,water} * c_{p,water} * \rho_{water} * (T_{out} - T_{in}) * \Delta t * \frac{1}{3600} \quad (3.\ 5)$$

3.2.4 Heat losses of the measurement box

In order to calculate the energy balance in a correct way, it is also important to consider the heat losses between the measurement box and the ambient. 20 cm rockwool insulation ($d_{rockwool}$) is used in order to reduce these losses.

The shape factor method is used to find heat losses. For a box geometry, it is used the shape factor taken from [24], defined as:

$$S = \frac{A}{d_{rockwool}} \quad (3.6)$$

Where A is the surface area of the box (1 m^2).

The heat losses $\Delta Q_{heatloss}$ [Wh] are given by:

$$\Delta Q_{heatloss} = \lambda * S * (T_{soil} - T_{ambient}) * \Delta t * \frac{1}{3600} \quad (3.7)$$

Where T_{soil} is the average temperature of the soil in each semicircle in the time step considered, S is the shape factor, Δt is the acquisition time and $\boldsymbol{\lambda}$ =0.037 W/mK is the thermal conductivity of the rockwool insulation material.

3.3 Results

In this section the main results obtained from the soil sample experiments are shown. The flow rate was set as low as possible in order to get a considerable different temperature between inlet and outlet in the inner pipe. The main results from the experiments are reported and discussed in the next paragraphs. Paragraph 3.3.1 concerns the charging operating mode (experiments with letter C), while paragraph 3.3.2 the discharging one (experiments with letter D). The analysis is done by taking into account different parameters: the heat exchange capacity rate, the power exchanged, the inlet – outlet temperature of the water, the overall heat transfer coefficient (H) and the pipe soil contact resistance (PSCR) in the heat transfer. In addition, heat balances are carried out in order to check that there is an equilibrium between the energy release, absorbed and lost by the soil sample and the water due to the interaction with the outer ambient.

3.3.1 Charge of the soil

In this first part of the results the charging operating mode is investigated. With the use of the electric boiler and the correct position of each valve, heated water is sent through the inner pipe in the soil sample in order to simulate the charge of the soil that could occur in the real facility when energy is sent from the collectors to the ground because the storage tank has already reached the required set temperature, or when the solar collectors produce water not warm enough to be sent to the tank, but still warmer than the soil temperature.

During the charging operating mode, water releases energy to the soil and part of it is lost or absorbed from the outer ambient. The charging operating mode is studied when the soil is warmer or colder than the outer ambient. When $T_{soil,initial} > T_{ambient}$, the energy balance is given by:

$$\Delta Q_{water} = \Delta Q_{soil,tot} + \Delta Q_{losses} \quad (3.\ 8)$$

When instead $T_{soil,initial} < T_{ambient}$ the energy balance is given by:

$$\Delta Q_{soil,tot} = \Delta Q_{water} + \Delta Q_{losses} \quad (3.\ 9)$$

With ΔQ_{water} = water energy content variation [Wh], $\Delta Q_{soil,tot}$ = total energy change of the soil [Wh] and ΔQ_{losses} = losses between the soil and the outer ambient [Wh].

Regarding the temperature of the soil ($T_{soil,initial}$), it is assumed an initial mean temperature of the soil ($T_{mean,initial,soil}$) calculated with the following equation, taking into account with a different weight the value of every circle temperature:

$$T_{mean,initial_{soil}} = 0.5 * T_{circle1} + 0.3 * T_{circle2} + 0.2 * T_{circle3} \quad (3.\ 10)$$

Where T_{circle_n} is the average value of the sensors of the n circle. $T_{circle1}$ has the bigger weight compared to the other circles because the thermocouples of circle 1 are the closest to the inner pipe.

For each experiment there is a table with the parameters used and obtained from the calculations and 2 graphs: the first for the HECR and the power, the second one for the energy balance.

In the next paragraphs the main results of the charging and discharging experiments are reported.

3.3.1.1 Experiment C1

Table 1 shows the mass flow rate, the average initial temperature of the soil, the inlet temperature and the average outlet temperature of the water in this first experiment regarding the charge of the soil. These data are measured for all the experiments. The HECR and the power exchanged, values calculated in each experiment, are also shown. The $HECR_{average}$ is 6.3 W/K, while the $power_{average}$ is 52 W. Flow rate is read from the flowmeter and it is converted from m^3/h to kg/s for the calculations. An average ΔT=0.5 K was obtained between inlet and outlet of the water flow in the soil box.

m [kg/s]	0.024
$T_{mean,initial,soil}$ [°C]	20.5
$T_{in,water}$ [°C]	29.0
$T_{out,water,average}$ [°C]	28.5
$HECR_{average}$ [W/K]	6.3
$Power_{average}$ [W]	52

Table 1: Experiment C1 input data

Figure 21 shows the trend of the HECR and of the power. The HECR has an initial value of 8 W/K and then it decreases reaching a constant value of around 6 W/K. The power has also a similar trend, with the maximum of 65 W at the start of the experiment, a minimum value of 45 W and an average value of 52 W.

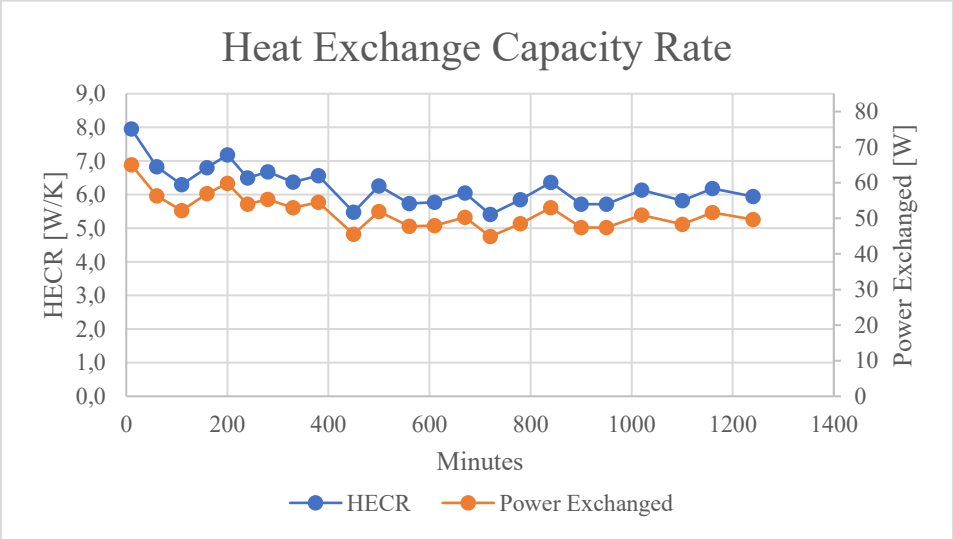

Figure 21: HECR and power exchanged, experiment C1.

Figure 22 shows the energy balance for experiment C1. The yellow curve (soil heat + heat losses) matches the blue curve, the heat releases by the water to the soil. The heat losses have a linear trend and they are about 17% of the energy absorbed by the soil.

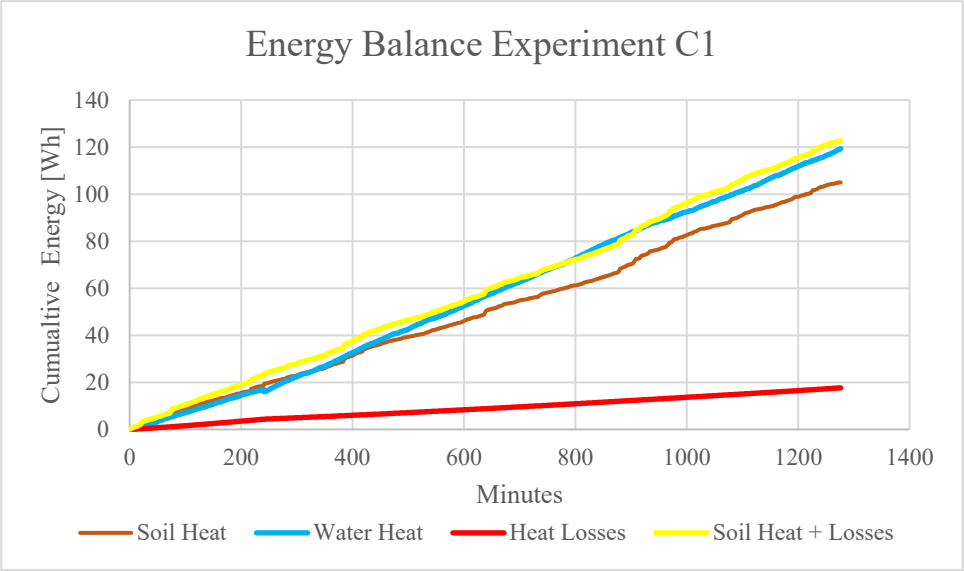

Figure 22: Energy balance experiment C1.

3.3.1.2 Experiment C2

Experiment C2 has similar input data ($T_{mean,initial,soil}$ and $T_{in,water}$ in Table 2) as experiment C1, in order to verify and compare the results. The $HECR_{average}$ is 5.8 W/K, slightly lower compared to experiment C1, while the average power is 58 W. An average ΔT = 0.6 K was obtained between inlet and outlet of the water flow.

m [kg/s]	0.024
$T_{mean,initial,soil}$ [°C]	20.7
$T_{in,water}$ [°C]	30.9
$T_{out,water,average}$ [°C]	30.3
$HECR_{average}$ [W/K]	5.8
$Power_{average}$ [W]	58

Table 2: Experiment C2 input data

Figure 23 shows the trend of the HECR and the power. The HECR has an initial value of 7.7 W/K and then it decreases reaching a constant value slightly lower than 6 W/K, similar to experiment C1. The power has also a similar trend, with the maximum of 75 W at the start of the experiment, a minimum value of 51 W and an average value of 58 W.

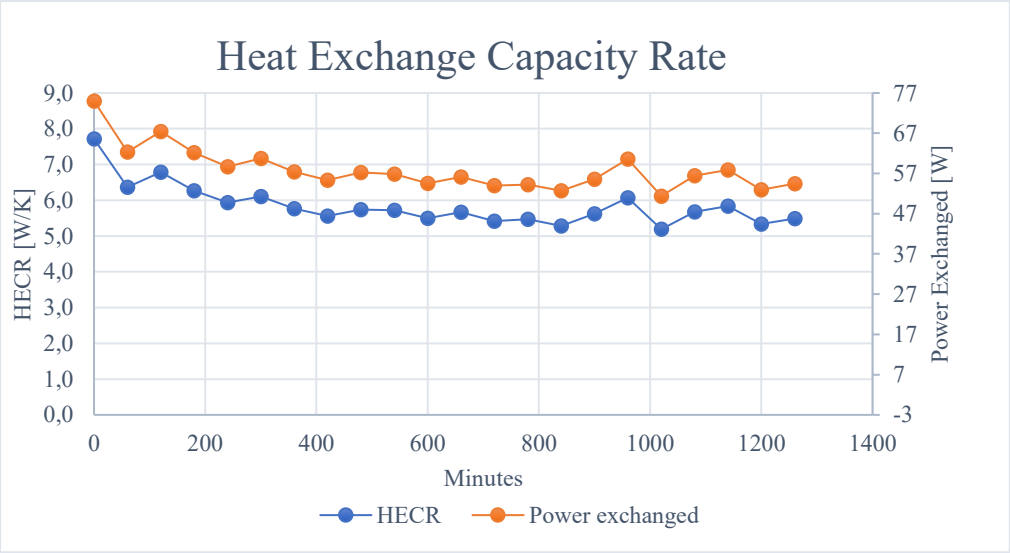

Figure 23: HECR and power exchanged, experiment C2.

Figure 24 shows the energy balance for experiment C2. Also in this case, the yellow curve (soil heat + heat losses) matches the blue curve, the heat releases by the water to the soil. The heat losses have a linear trend and they are about 18% of the energy absorbed by the soil.

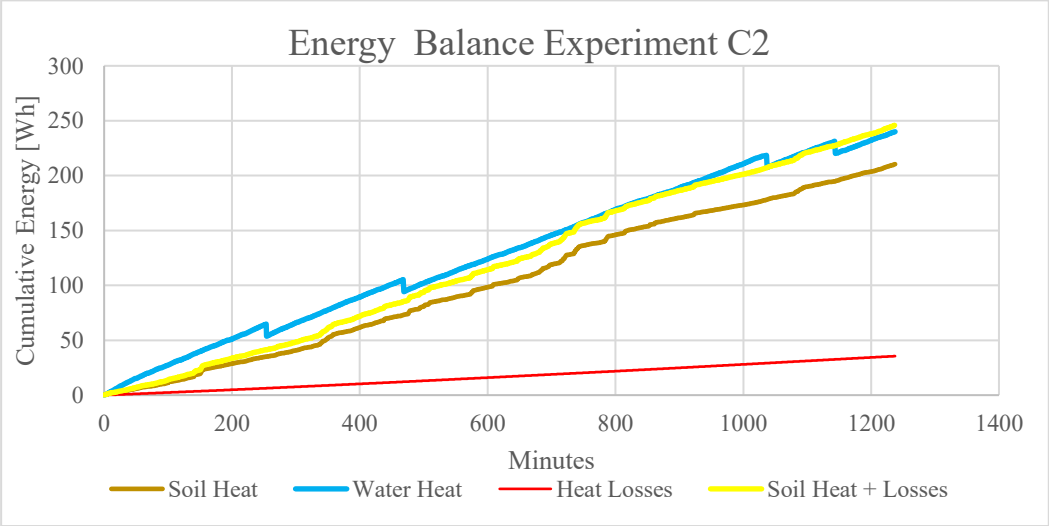

Figure 24: Energy balance experiment C2.

3.3.1.3 Experiment C3

Experiment C3 has input data ($T_{mean,initial,soil}$ and $T_{in,water}$ in Table 3) higher than the 2 previous experiments, in order to investigate the trend of the HECR and of the power in another operating temperature range. The $HECR_{average}$ obtained is 5.6 W/K while the average power is 62 W. The ranges of temperatures of the soil and of the water in this experiment want to simulate a possible charging operation condition of the soil during a summer month, when the real temperature of the

soil can be more than 20 °C and the solar collectors produce water at 35 °C. An average ΔT= 0.7 K was obtained between inlet and outlet of the water flow.

m [kg/s]	0.022
$T_{mean,initial,soil}$ [°C]	22.6
$T_{in,water}$ [°C]	34.6
$T_{out,water,average}$ [°C]	33.9
$HECR_{average}$ [W/K]	5.6
$Power_{average}$ [W]	62

Table 3: Experiment C3 input data.

Figure 25 shows the trend of the HECR and the power. The HECR has an initial value of 7.4 W/K and then it decreases reaching a constant value of around 5 W/K. The power has also a similar trend, with the maximum of 88 W at the start of the experiment and a minimum value of 58 W.

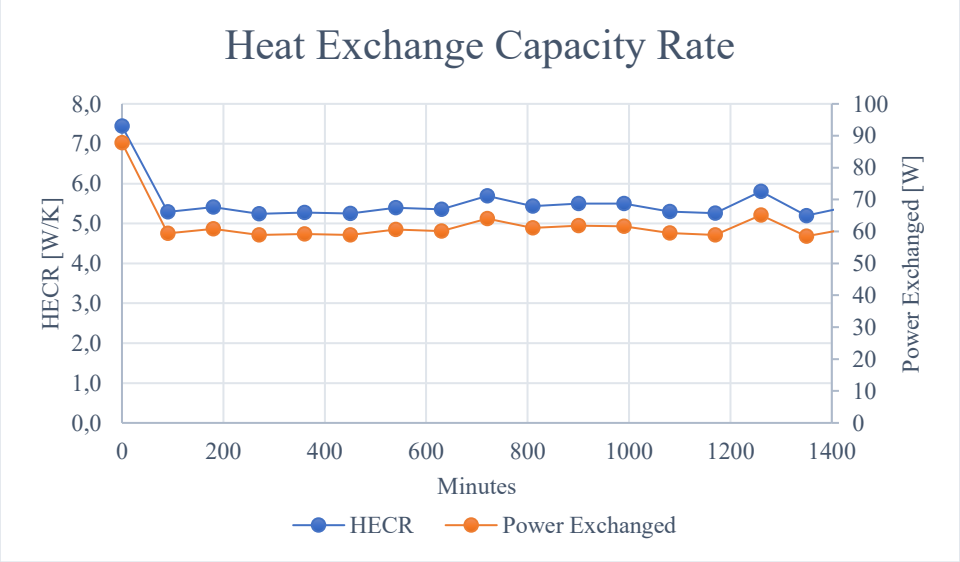

Figure 25: HECR and power exchanged, experiment C3.

Figure 26 shows the energy balance for experiment C3. Also in this case, the yellow curve (soil heat + heat losses) matches the blue curve, the heat releases by the water to the soil. The heat losses have a linear trend and they are about 17% of the energy absorbed by the soil.

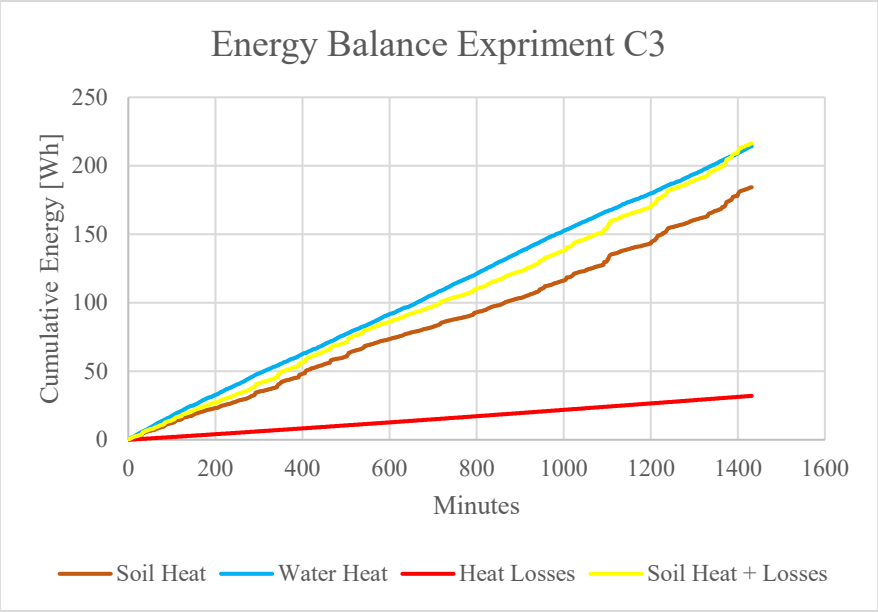

Figure 26: Energy balance experiment C3.

3.3.1.4 Experiment C4

Experiment C4 has similar input data ($T_{mean,initial,soil}$ and $T_{in,water}$ in Table 4) as experiment C3. The $HECR_{average}$ is 5.4 W/K, slightly lower compared to experiment C3, while the average power is 58 W. An average $\Delta T = 0.7$ K was obtained between inlet and outlet of the water flow.

m [kg/s]	0.021
$T_{mean,initial,soil}$ [°C]	22.5
$T_{in,water}$ [°C]	34.5
$T_{out,water,average}$ [°C]	33.8
$HECR_{average}$ [W/K]	5.4
$Power_{average}$ [W]	58

Table 4: Experiment C4 input data.

Figure 27 shows the trend of the HECR and the power. The HECR has an initial value of 6.3 W/K and then it decreases reaching a constant value of around 5 W/K, similar to experiment C3. The power has also a similar trend, with the maximum of 72 W at the start of the experiment and a minimum value of 57 W.

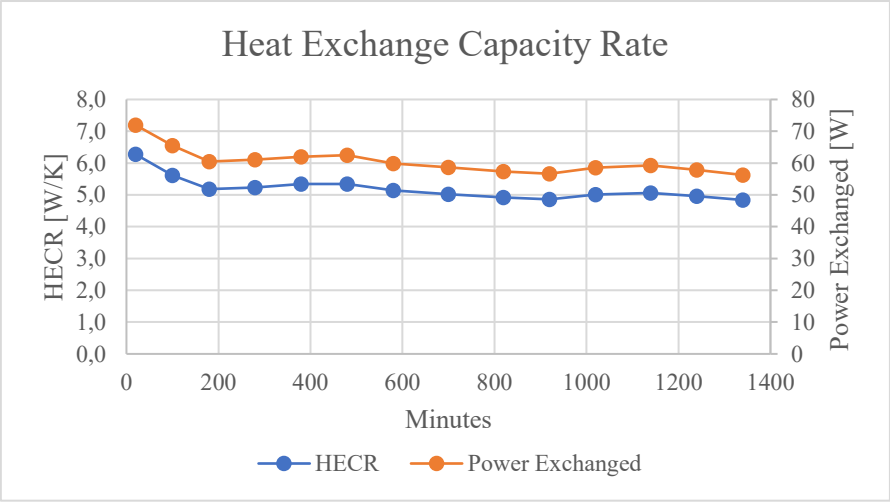

Figure 27: HECR and power exchanged, experiment C4.

Figure 28 shows the energy balance for experiment C4. Also in this case, the yellow curve (soil heat + heat losses) matches the blue curve, the heat releases by the water to the soil. The heat losses have a linear trend and they are about 14% of the energy absorbed by the soil.

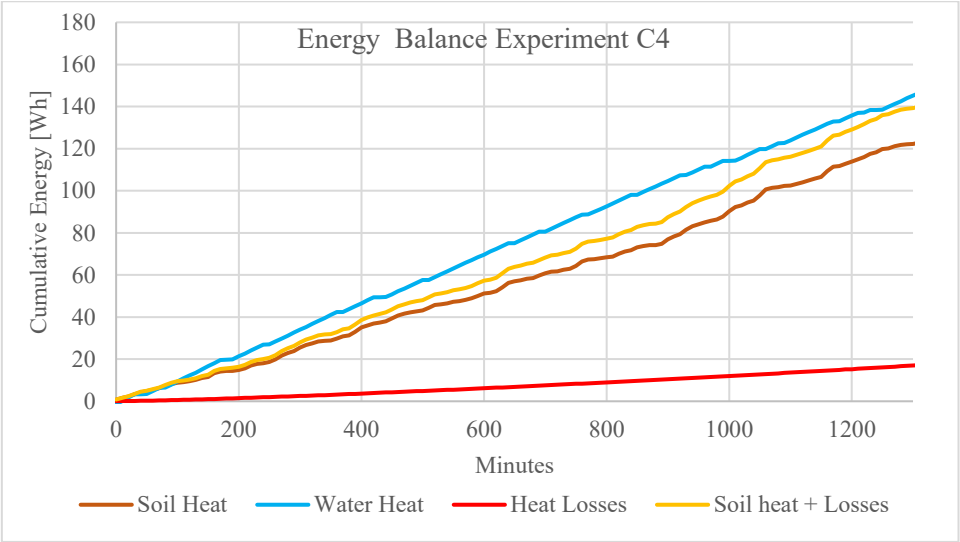

Figure 28: Energy balance experiment C4.

3.3.1.5 Experiment C5

Experiment C5 has higher input data ($T_{mean,initial,soil}$ = 27 °C and $T_{in,water}$ = 39.1 °C in Table 5) compared to the previous experiments. This situation could occur during summer days in July or August when the solar collectors provide water up to 40 °C, the heating demand of the storage tank is low and the solar radiation leads to high T_{soil}. The $HECR_{average}$ is 6 W/K, while the average power is 73 W. An average ΔT = 0.7 K was obtained between inlet and outlet of the water flow.

m [kg/s]	0.023
$T_{mean,initial,soil}$ [°C]	27
$T_{in,water}$ [°C]	39.1
$T_{out,water,average}$ [°C]	38.4
$HECR_{average}$ [W/K]	6
$Power_{average}$ [W]	73

Table 5: Experiment C5 input data

Figure 29 shows the trend of the HECR and the power. The HECR has an initial value of 7.7 W/K and then it decreases reaching a constant value of around 6 W/K. The power has also a similar trend, with the maximum of 89 W at the start of the experiment and a minimum value of 66 W.

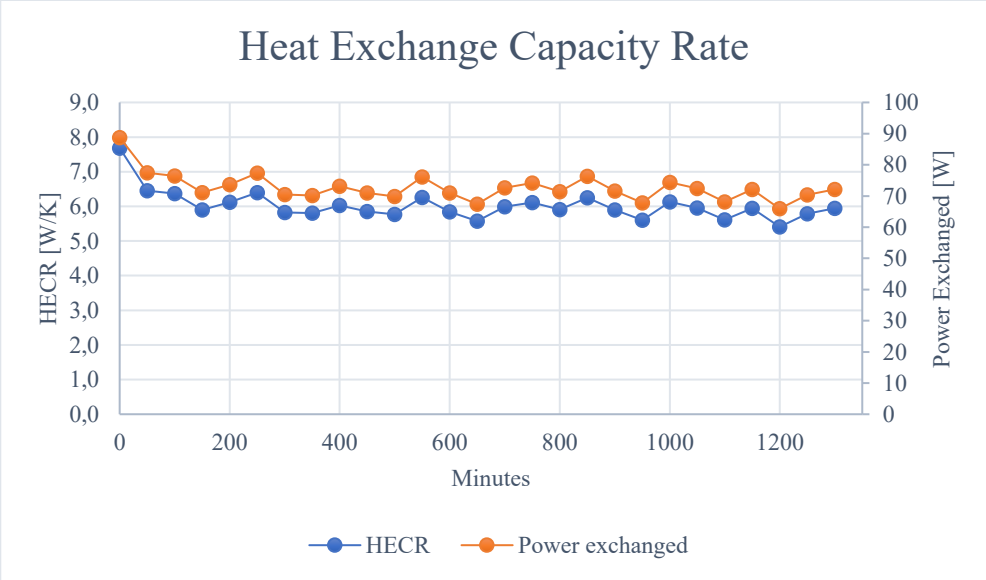

Figure 29: HECR and power exchanged, experiment C5.

Figure 30 shows the energy balance for experiment C5. In this case, the yellow curve (soil heat + heat losses) matches the blue curve, the heat released by the water to the soil. The difference between T_{soil} = 27°C and the ambient temperature is higher in this experiment and thus the heat losses are about 28% of the energy absorbed by the soil and they have a linear trend.

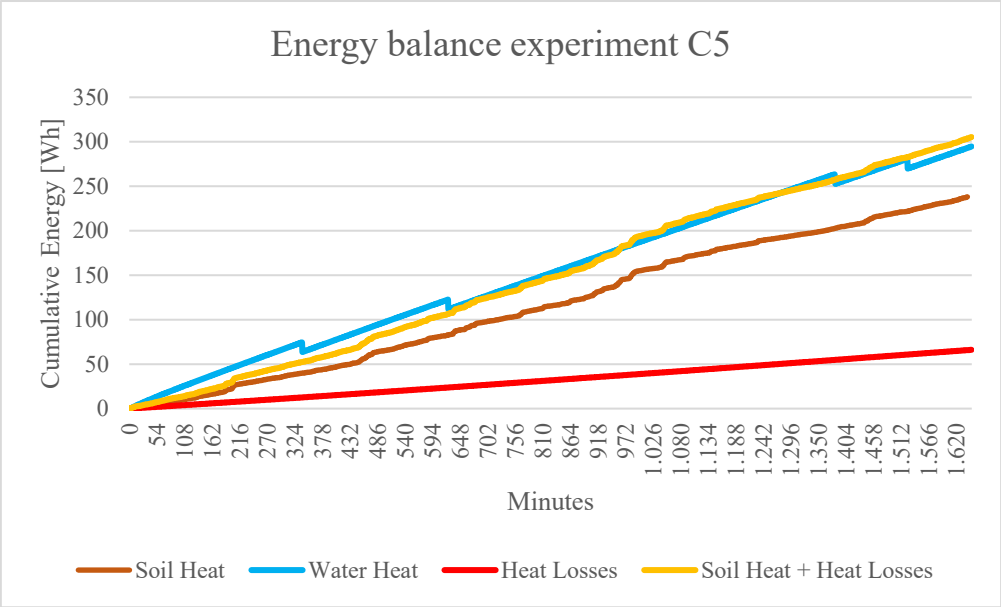

Figure 30: Energy balance experiment C5.

3.3.1.6 Experiment C6

Experiment C6 has similar input data (Table 6) as experiment C5, just T_{soil} = 19.8 °C is much lower compared to the previous experiment in order to analyse another range of operation regarding the charge of the soil. The $HECR_{average}$ is 5.6 W/K, lower compared to experiment C5, while the average power is 65 W. An average ΔT = 0.6 K was obtained between inlet and outlet of the water flow.

m [kg/s]	0.022
$T_{mean,initial,soil}$ [°C]	19.8
$T_{in,water}$ [°C]	34.5
$T_{out,water,average}$ [°C]	33.9
$HECR_{average}$ [W/K]	5.6
$Power_{average}$ [W]	65

Table 6: Experiment C6 input data.

Figure 31 shows the trend of the HECR and the power. The HECR has an initial value of 6.2 W/K and then it decreases reaching a constant value of around 5.5 W/K. The power has also a similar trend, with the maximum of 72 W at the start of the experiment and a minimum value of 60 W.

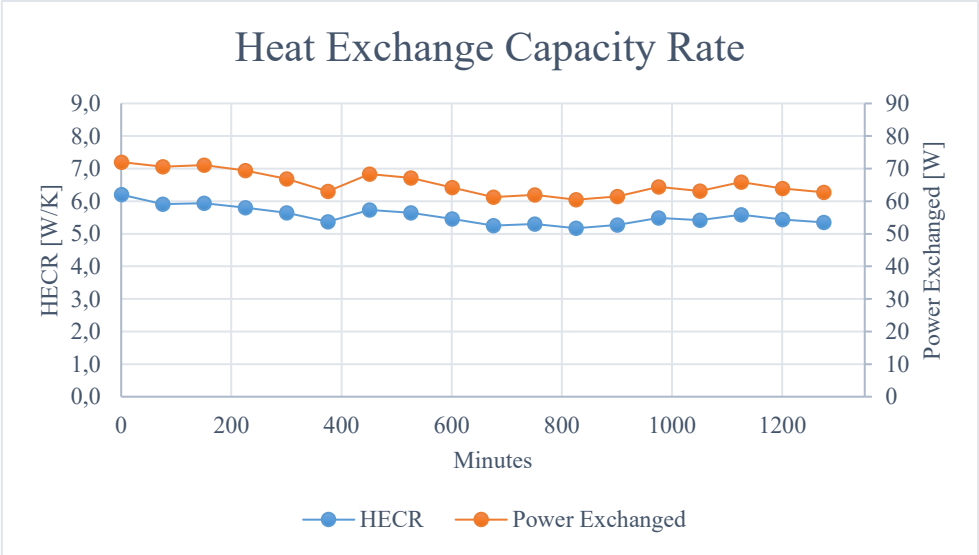

Figure 31: HECR and power exchanged, experiment C6.

Figure 32 shows the energy balance for experiment C6. Also in this case, the yellow curve (soil heat + heat losses) matches the blue curve, the heat releases by the water to the soil. The heat losses have a linear trend and they are about 21% of the energy absorbed by the soil.

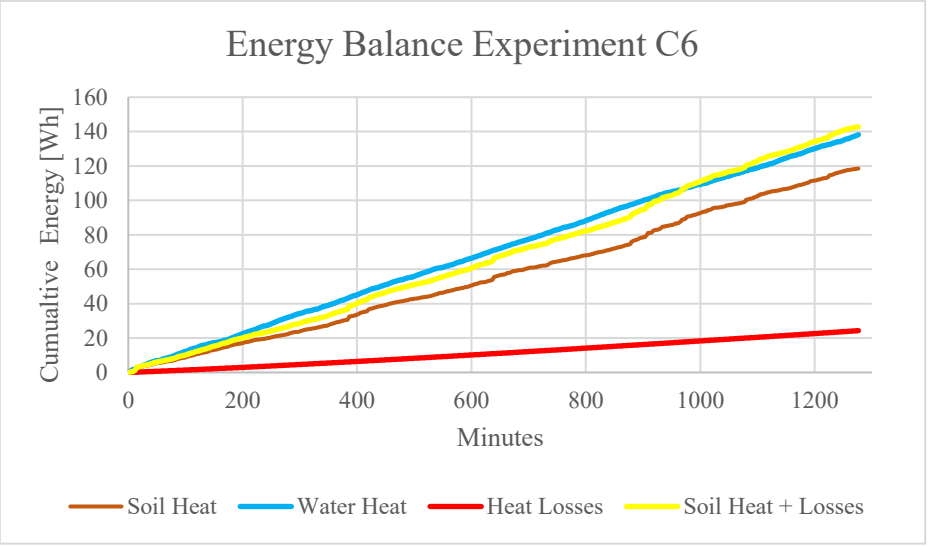

Figure 32: Energy balance experiment C6.

3.3.1.7 Experiment C7

Experiment C7 has input data (Table 7) different from the other experiments. Indeed the soil sample has been cooled down until T_{soil} = 12°C before the experiment was performed, then water at 21.8 °C was sent through the inner pipe. The $HECR_{average}$ is 5.3 W/K, lower compared to the other cases, while the average power is 51 W. An average ΔT = 0.7 K was obtained between inlet and outlet of the water flow.

m [kg/s]	0.022
$T_{mean,initial,soil}$ [°C]	12
$T_{in,water}$ [°C]	21.8
$T_{out,water,average}$ [°C]	21.1
$HECR_{average}$ [W/K]	5.3
$Power_{average}$ [W]	51

Table 7: Experiment C7 input data.

Figure 33 shows the trend of the HECR and the power. The HECR has an initial value of 8 W/K and then it decreases reaching a constant value of around 4.5 W/K, lower compared to the previous results. The power exchanged has the maximum of 76 W at the start of the experiment and a minimum value of 45 W.

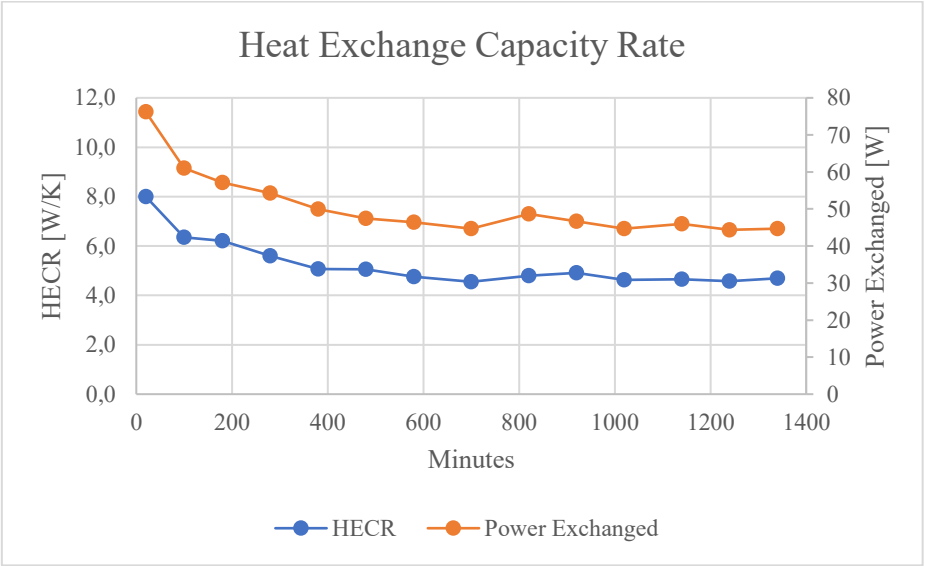

Figure 33: HECR and power exchanged, experiment C7.

Figure 34 shows the energy balance for experiment C7. In this case, the yellow curve (water heat + heat losses) matches the brown curve, the heat releases by the soil to the water and the ambient (energy balance given by equation 3.9). The heat losses have a linear trend and they are about 24% of the energy absorbed by the water. This value is higher compared to some of the previous experiments because the temperature difference between soil and ambient has increased (T_{soil} = 12°C and $T_{ambient}$ = 22°C).

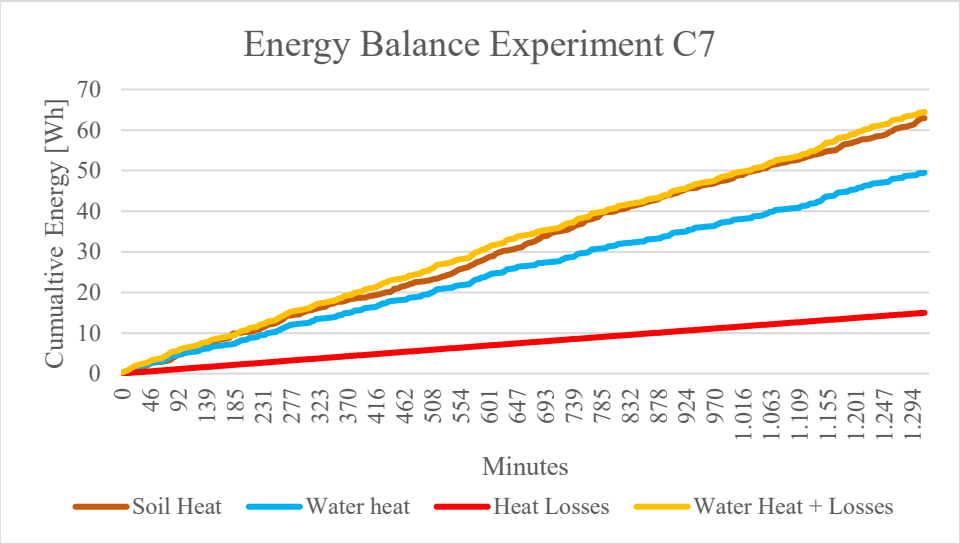

Figure 34: Energy balance experiment C7.

An analysis regarding the previous results, the HTC and the PSCR is done in paragraph 3.4 .

3.3.2 Discharge of the soil

In this second part of the results, the discharging operating mode is investigated. For each experiment is reported a table with the parameters used and obtained, the trend regarding the HECR, the power exchanged and the heat balance. The method used is the same as the charging operating mode experiments.

By using the cooling system of the laboratory and by adjusting in the correct position each valve for the discharging mode, cold water is sent through the inner pipe in the soil sample in order to simulate the discharge of the soil that could occur in the real facility when the heat pump is in operation and the heat flux goes from the ground to the ground loop fluid and then to the tank in the facility. Cold water can be sent also in the two radiators if the soil sample needs to be cooled.

The cooling fluid is provided by the DTU cooling system. It goes inside a plate heat exchanger where it absorbs heat from the water of the closed loop that goes through the inner pipe for the experiments.

Temperature of the cooling fluid that absorbs heat from the water of the close loop can be monitored by a throttle valve controlled by a voltage signal directly sent by LabView software to the valve. The voltage range is 0 – 5 V: 0 means valve fully closed (no flow of the cooling fluid in the plate heat exchanger), 5 V means valve full open (maximum flow of the cooling fluid in the plate heat exchanger). The temperature is set with a specific value in the setpoint cell visible in

Figure 35 (red circle) and the throttle valve will open or close depending of the temperature set. In [25] more information regarding the Labview control system can be found.

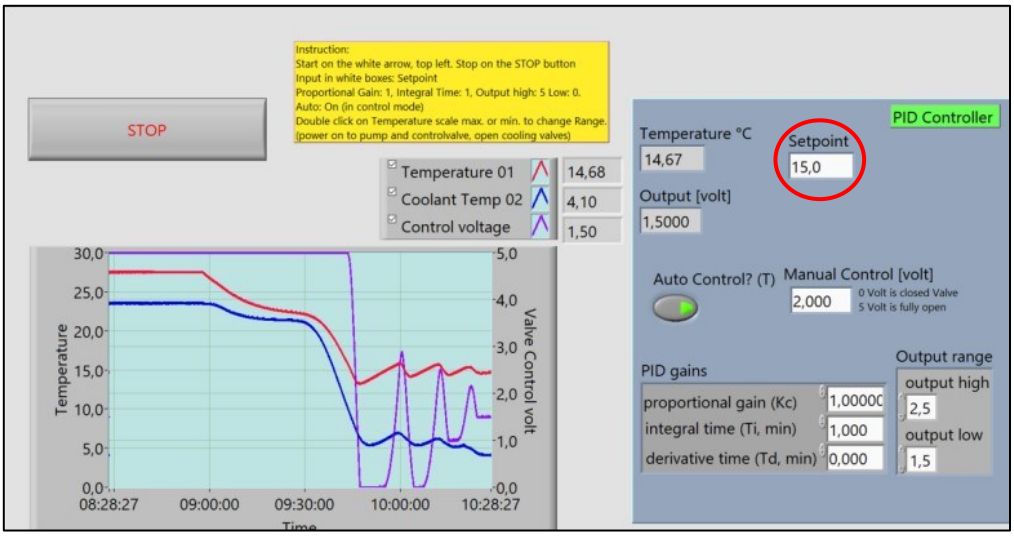

Figure 35: Labview control system to set the inlet temperature of the cooling fluid during the discharge of the soil.

During the discharging operating mode, energy is absorbed by the water from the soil.

Considering the energy balance, it must be verified that:

$$\Delta Q_{heatlosses} + \Delta Q_{water} = \Delta Q_{soil,tot} \qquad (3.\ 11)$$

With ΔQ_{water} = water energy content variation [Wh], $\Delta Q_{soil,tot}$ = total energy change of the soil [Wh] and $\Delta Q_{heatlosses}$ = losses between the soil and the outer ambient [Wh].

The same assumptions regarding the average initial soil temperature $T_{mean,initial,soil}$ explained with equation 3.10 are used for the discharging of the soil.

3.3.2.1 Experiment D1

Table 8 shows the temperatures of the soil and of the water in this first experiment regarding the discharge of the soil. The mass flow rate, the HECR and the power exchanged are also shown. The $HECR_{average}$ is 3.4 W/K, while the average power is 29 W. An average $\Delta T = 2$ K was obtained between inlet and outlet of the water flow in all the discharge experiments.

m [kg/s]	0.017
$T_{mean,initial,soil}$ [°C]	22
$T_{in,water}$ [°C]	6
$T_{out,water,average}$ [°C]	8
$HECR_{average}$ [W/K]	3.4
$Power_{average}$ [W]	29

Table 8: Experiment D1 input data.

Figure 36 shows the trend of the HECR and the power. The HECR has an initial value of 3.2 W/K and then it reaches a constant value of around 3.5 W/K. The power has a maximum of 34 W and a minimum of 26 W. Already from this first discharge experiment, it is visible a clear difference with the charge experiments, with lower values of HECR and power exchanged.

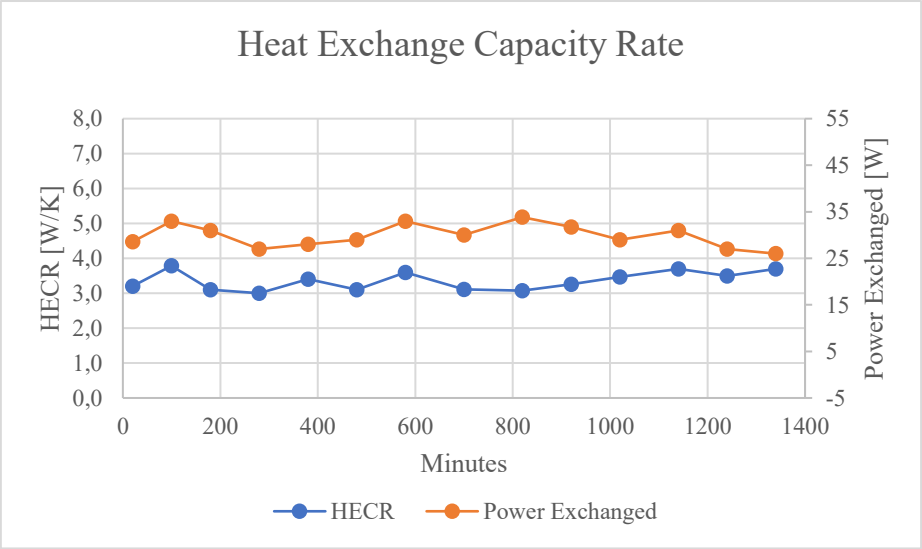

Figure 36: HECR and power exchanged, experiment D1.

Figure 37 shows the energy balance for experiment D1. In this case, the yellow curve (soil heat - heat losses) matches the blue curve, the heat absorbed by the water (energy balance given with equation 3.12). The heat losses have a linear trend and they are about 10% of the energy absorbed by the water.

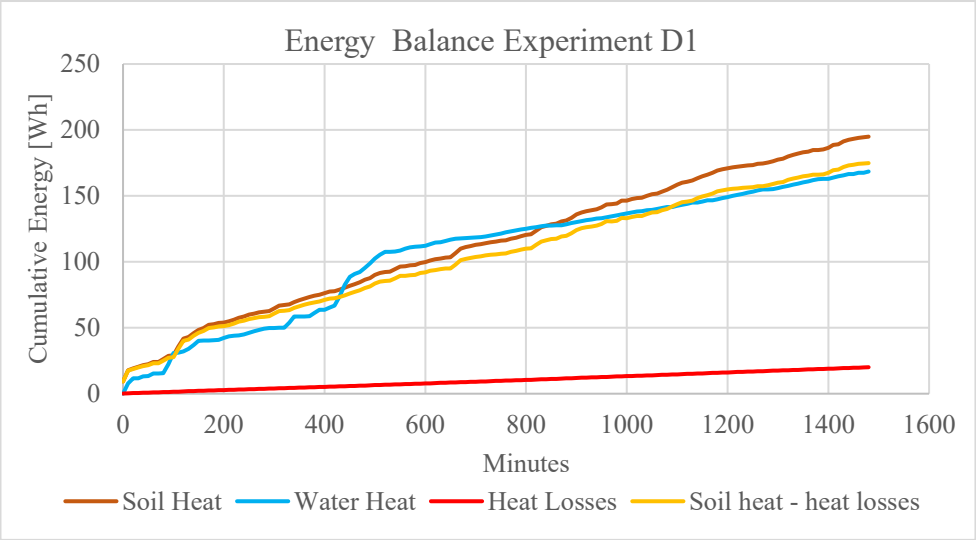

Figure 37: Energy balance experiment D1.

3.3.2.2 Experiment D2

Table 9 shows the temperatures of the soil and of the water in this second experiment regarding the discharge of the soil: results are similar to the previous one that has same initial values. The $HECR_{average}$ is 3.6 W/K, while the average power is 33 W.

m [kg/s]	0.017
$T_{mean,initial,soil}$ [°C]	22.5
$T_{in,water}$ [°C]	6
$T_{out,water,average}$ [°C]	8
$HECR_{average}$ [W/K]	3.6
$Power_{average}$ [W]	33

Table 9: Experiment D2 input data.

Figure 38 shows the trend of the HECR and the power. The HECR has an initial value of 3.5 W/K and the power of 46 W. The minimum power is 37 W and the maximum 46 W.

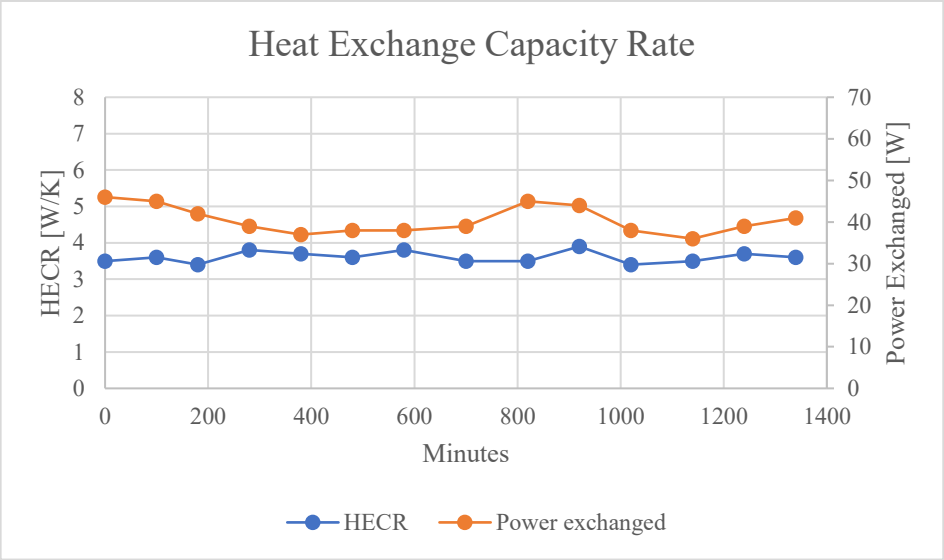

Figure 38: HECR and power exchanged experiment D2.

Figure 39 shows the energy balance for experiment D2. In this case, the yellow curve (soil heat - heat losses) matches the blue curve, the heat absorbed by the water. The heat losses have a linear trend and they are about 12% of the energy absorbed by the water.

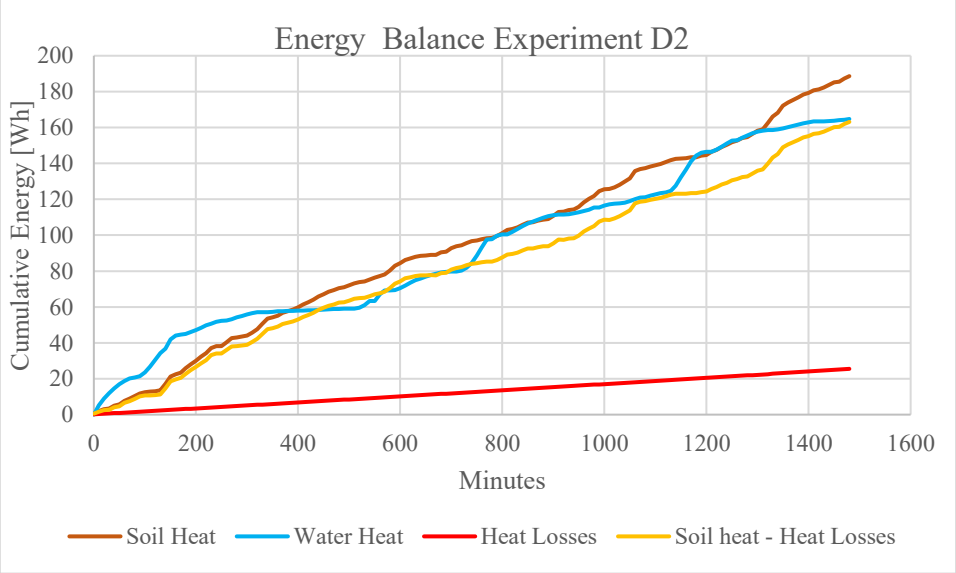

Figure 39: Energy balance experiment D2.

3.3.2.3 Experiment D3

Table 10 shows the temperatures of the soil and of the water in this third experiment regarding the discharge of the soil. The soil sample has been cooled down until $T_{mean,initial,soil}$ = 15°C in order to simulate another operating situation compared to the previous experiments, also the inlet temperature of the water is lower compared to the previous cases. The mass flow rate, the HECR

and the power exchanged are also shown. The $HECR_{average}$ is 4.3 W/K, while the average power is 44 W.

m [kg/s]	0.014
$T_{mean,initial,soil}$ [°C]	15
$T_{in,water}$ [°C]	4
$T_{out,water,average}$ [°C]	6
$HECR_{average}$ [W/K]	4.3
$Power_{average}$ [W]	44

Table 10: Experiment D3 input data.

Figure 40 shows the trend of the HECR and the power. The HECR has an initial value of 6 W/K and the power of 65 W. Both the HECR and the power exchanged decrease and reach constant values of around 4 W/K and 40 W.

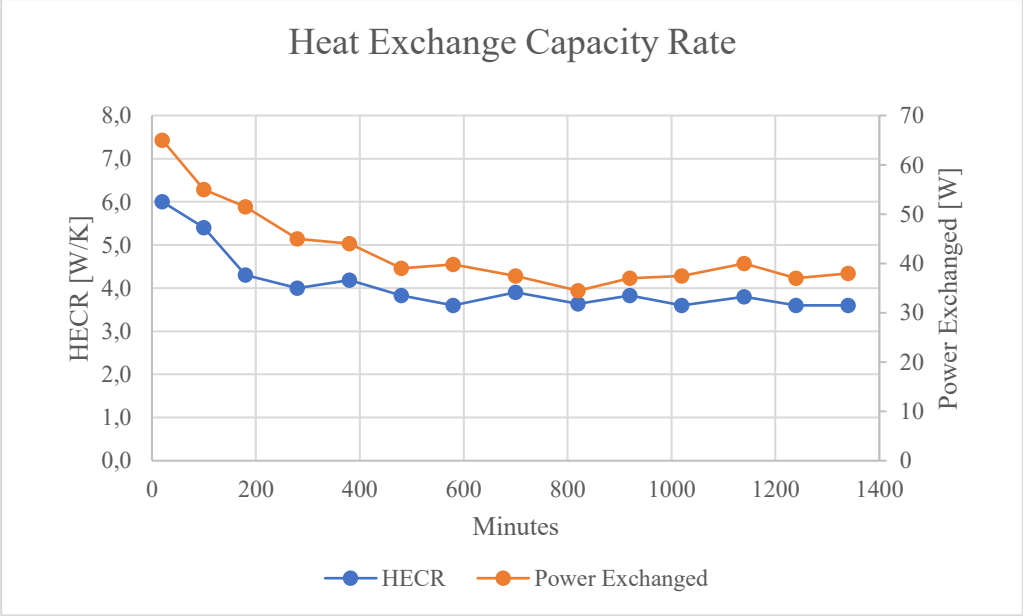

Figure 40: HECR and power exchanged, experiment D3.

Figure 41 shows the energy balance for experiment D3. The yellow curve (soil heat - heat losses) matches the blue curve, the heat absorbed by the water. The heat losses have a linear trend and they are about 14% of the energy absorbed by the water.

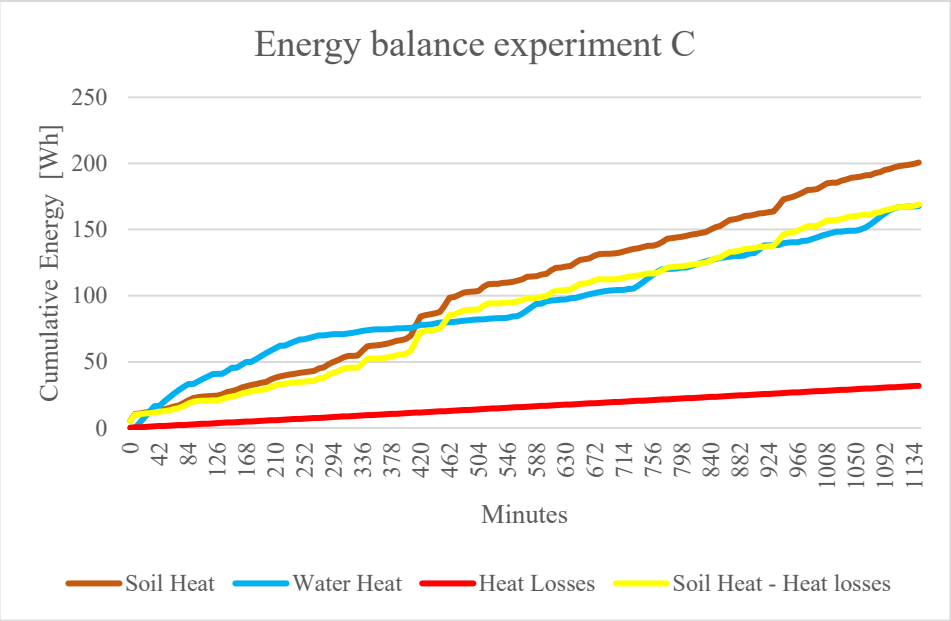

Figure 41: Energy balance experiment D3.

3.3.2.4 Experiment D4

Table 11 shows the temperatures of the soil and of the water in this last experiment. The soil sample has been cooled down until $T_{mean,initial,soil}$ = 13.7°C in order to simulate another operating situation compared to the previous experiments, also the inlet temperature of the water is lower compared to the previous cases. The mass flow rate, the HECR and the power exchanged are also shown. The $HECR_{average}$ is 4.1 W/K, while the average power is 42 W.

m [kg/s]	0.014
$T_{mean,initial,soil}$ [°C]	13.7
$T_{in,water}$ [°C]	1.7
$T_{out,water,average}$ [°C]	2.3
$HECR_{average}$ [W/K]	4.1
$Power_{average}$ [W]	42

Table 11: Experiment D4 input data

Figure 42 shows the trend of the HECR and the power. The HECR has an initial value of 4.3 W/K and the power of 49 W. Both the HECR and the power exchanged have a constant trend during the experiment with small variation around their average value.

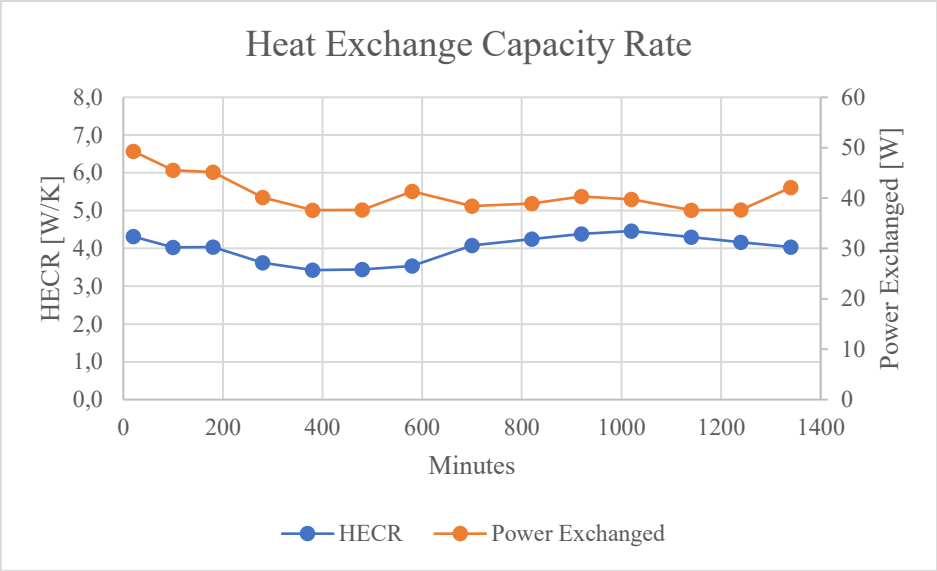

Figure 42: HECR and power exchanged experiment D4.

Figure 43 shows the energy balance for experiment D4. The yellow curve (soil heat - heat losses) matches the blue curve, the heat absorbed by the water. The heat losses have a linear trend and they are about 25% of the energy absorbed by the water.

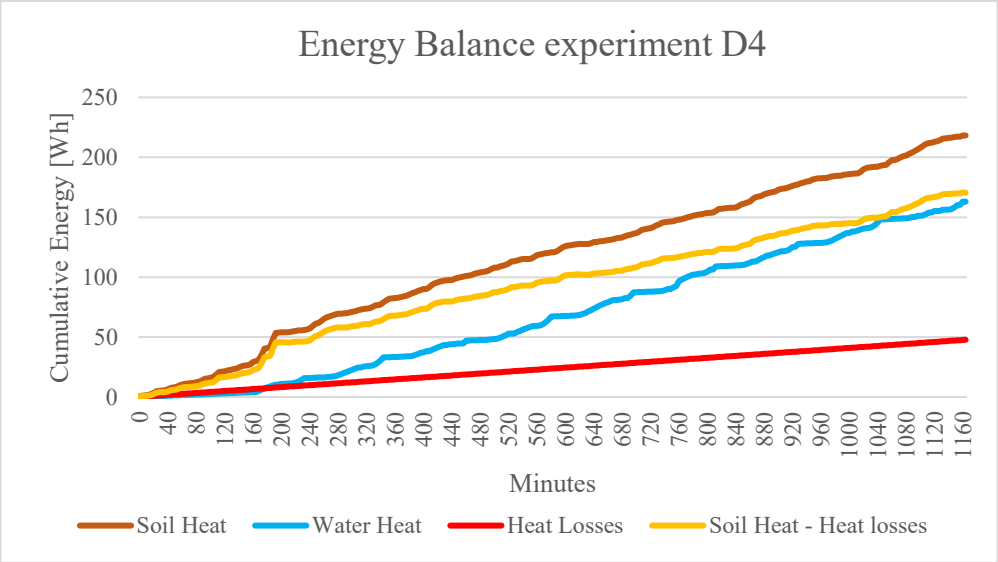

Figure 43: Energy balance experiment D4.

3.3.3 HTC analysis

In this paragraph, an analysis regarding the heat transfer coefficients (HTC) is carried out. The overall heat transfer coefficient (H), the heat transfer coefficient on the inner side of the pipe ($h_{c,i}$) and the heat transfer coefficient on the outer side of the pipe ($h_{c,o}$) are considered. It is investigated how these parameters vary with different operating conditions in the experiments (charging or discharging of the soil sample).

The overall heat transfer coefficient is calculated for each timestep by knowing the power exchanged P [W], the inner side area of the pipe A_{in} [m^2] and logarithmic mean temperature difference $\Delta T_{logaritmic}$ [K] between the soil temperature and the inlet – outlet temperatures of the water. The overall heat transfer coefficient H [W/m^2K] is given by:

$$H = \frac{P}{A_{in} * \Delta T_{logaritmic}} \quad (3.\ 12)$$

The inner heat transfer coefficient $h_{c,i}$ [W/m^2K] can be instead calculated by considering the following experimental equations taken from [26]:

$$Nu = 0.016 * Pr_m^{0.34} * Re^{0.82} * \left(\frac{Pr_m}{Pr_w}\right)^{0.25} \quad (3.\ 13)$$

Where Pr_m is the Prandtl number of the water at the mean temperature between inlet and outlet, while Pr_w is the Prandtl number of the water at the inlet temperature. Nusselt, Reynolds and Prandtl numbers can be also expressed as:

$$Nu = \frac{h_{c,i} * 2 * r_i}{\boldsymbol{\lambda_s}} \quad (3.\ 14)$$

$$Re = \frac{v * 2 * r_i}{v_s} \quad (3.\ 15)$$

$$Pr = \frac{c_p * \mu}{k} \quad (3.\ 16)$$

Where r_i is the inner radius of the pipe, $\boldsymbol{\lambda}_s$ is the thermal conductivity of the water [W/mK], v_s is the kinematic viscosity of the water [m^2/s], v is the velocity of the water in the pipe [m/s], c_p is the specific heat of water [J/kgK], μ is the dynamic viscosity [Pa*s] and k is the thermal conductivity [W/mk].

The overall heat transfer coefficient takes into account all the resistances that influence the heat transfer process in each experiment: the resistance between fluid and inner side of the pipe, the resistance of the pipe and the resistance between soil and outer side of the pipe. It can be also express as function of these 3 resistances with the following equation taken from [26]:

$$H = \frac{1}{\left(\frac{1}{2*\Pi*r_i*L*h_{c,i}} + \frac{\ln\frac{r_y}{r_i}}{2*\Pi*\boldsymbol{\lambda}_{spiral}*L} + \frac{1}{2*\Pi*r_y*L*h_{c,o}}\right)} \qquad (3.17)$$

Where r_i is the inner radius of the pipe [m], L is the length of the pipe [m], $h_{c,i}$ is the inner heat transfer coefficient [W/m^{2}K], r_y is the outer radius of the pipe [m], $\boldsymbol{\lambda}_{spiral}$ is the thermal conductivity of the pipe material [W/mK] and $h_{c,o}$ is the outer heat transfer coefficient [W/m^{2}K]. The first term in the denominator of the above equation is the resistance in the inner side, the second one the pipe material resistance and the third one the resistance of the outer side.

By knowing H and $h_{c,i}$ with equations 3.12 and 3.14, it is possible to find $h_{c,o}$ with equation 3.17.

In Figure 44 the overall heat transfer coefficient trend is shown for each experiment. The red dot line divides the plots in two parts: above it there is the H for charging operating experiments, below it for the discharging operating experiments. There is a clear different in the overall heat transfer coefficient between the two different operating mode.

The average value of H for the charge of the soil is H_C = 147 W/m^{2}K, while for discharging the soil is H_D = 78 W/m^{2}K. This means that the heat transfer better occurs when the water releases heat to the soil during the charging operating mode compared to the discharging one, with reference to the temperature ranges considered in the experiments.

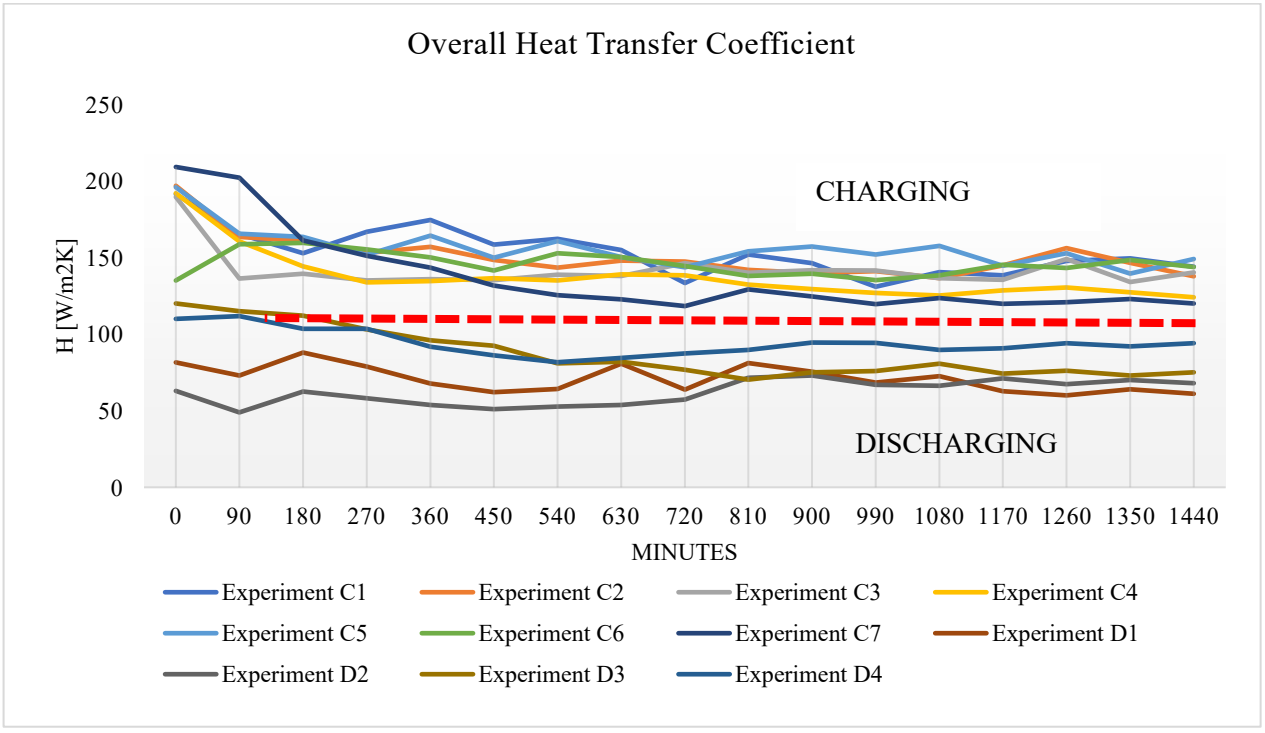

Figure 44: Overall heat transfer coefficient (H) trends in each experiment.

It is also interesting to analyse the overall heat transfer coefficient considering the inner heat transfer coefficient ($h_{c,i}$) and the outer heat transfer coefficient ($h_{c,o}$). Figure 45 shows the final results for each experiment, highlighting a bigger value of $h_{c,i}$ (orange bars) compared to $h_{c,o}$ (grey bars), both during the charge and the discharge of the soil. This means that the resistance on the inner side of the pipe is lower compared to the outer side. Also, the lower mass flow rate in the discharge experiments influences just the inner heat transfer coefficient ($h_{c,i}$) that is indeed lower in the discharge process than in the charge process, but it does not influence the outer heat transfer coefficient ($h_{c,o}$).

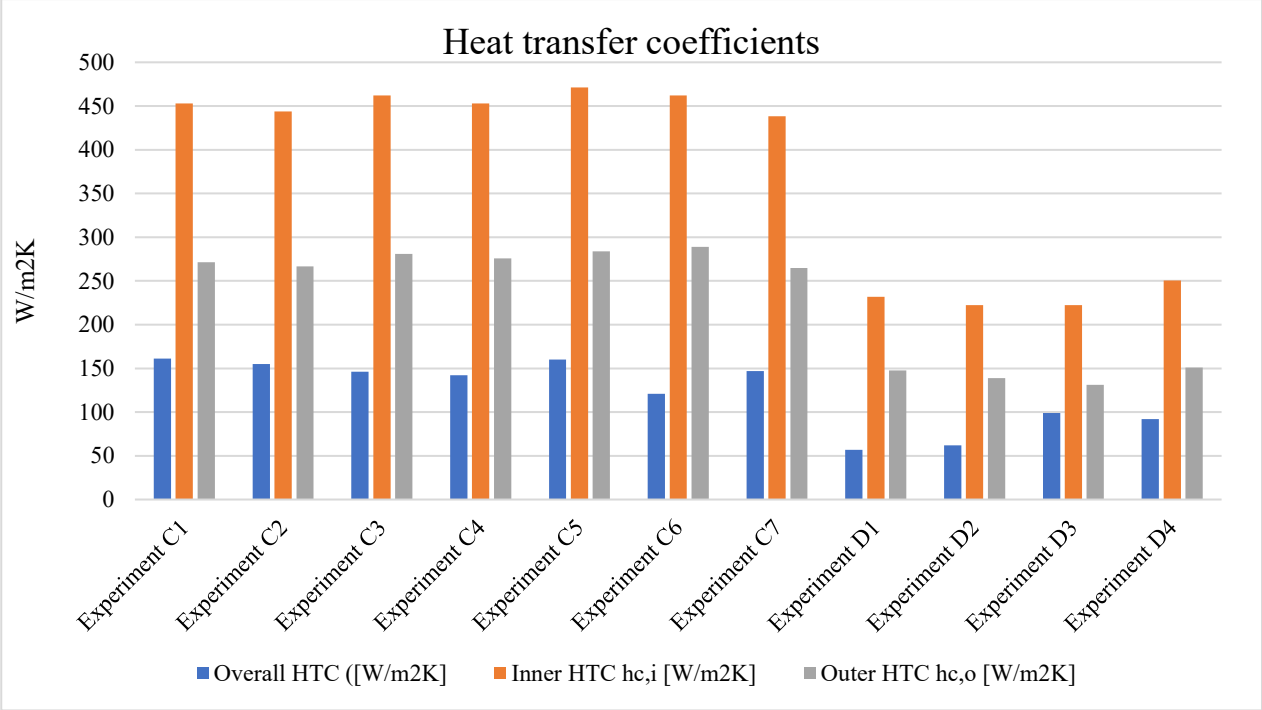

Figure 45: Heat transfer coefficients for each experiment.

3.4 Discussion of the results regarding the soil sample experiments

The soil sample experiments performed aim to better understand the heat transfer between water and soil with different operating conditions (charge – discharge) and different temperature ranges. Table 12 reports the main results for each experiment: the overall heat transfer coefficient (H), the inner heat transfer coefficient ($h_{c,i}$), the outer heat transfer coefficient ($h_{c,o}$), the average inlet temperature of the water in the pipe ($T_{water,inlet}$), the initial temperature of the soil ($T_{soil,initial}$), the HECR and the PSCR are shown.

By taking into consideration the HECR and the overall heat transfer coefficient for each experiment, the charge of the soil has the highest results compared to the discharge of the soil, meaning that the heat transfer better occurs in this operating mode. The HECR varies between 5.3

W/K and 6.3 W/K in the charging operating mode, while between 3.4 W/K and 4.3 W/K in the discharging operating mode. Regarding the overall heat transfer coefficient, it varies between 121 W/m^2K and 161 W/m^2K in the charging operating mode, while between 57 W/m^2K and 99 W/m^2K in the discharging operating mode.

The inner HTC ($h_{c,i}$) is higher in the charging experiment compared to the discharging ones, but it must be taken into consideration that this value depends on the mass flow rate, which is lower in the discharging experiments. Instead, the outer HTC ($h_{c,o}$), which does not depend on the mass flow rate, is higher in the charging experiment because of the thermal expansion of the pipe that goes inside the soil sample due to the high temperature of operation, meaning a better contact between soil and outer side of the pipe.

In the table below the thermal resistance is also listed and it is defined as the inverse of the overall heat transfer coefficient. It considers the inner side resistance, the pipe material resistance and the outer resistance, as shown with equation 3.18. It has the smallest value in the charging operating mode with an average of $PSCR_{C,average} = 0.007\ m^2K/W$, indeed the heat transfer better occurs in this case; in the discharging operating mode instead the average value is $PSCR_{D,average} = 0.013\ m^2K/W$.

SUMMARY											
	CHARGING OF THE SOIL							DISCHARGING			
Experiment	C1	C2	C3	C4	C5	C6	C7	D1	D2	D3	D4
Mass flow rate [m^3/s]	0.024	0.024	0.022	0.021	0.023	0.022	0.022	0.014	0.014	0.014	0.014
H [W/m2K]	161	155	146	142	160	121	147	57	62	99	92
Twater,inlet [°C]	29	31	35	35	35	35	22	6	6	4	2
Tsoil,initial [°C]	20	21	22.6	22.5	19.8	19.8	12	22	22.5	15	13
HECR [W/K]	6.3	5.8	5.6	5.5	6	5.6	5.3	3.4	3.6	4.3	4
Thermal Resistance [m^2K/W]	**0.006**	**0.006**	**0.007**	**0.007**	**0.006**	**0.008**	**0.007**	**0.018**	**0.016**	**0.010**	**0.011**

Table 12: Summary of the experiments performed regarding the soil sample.

Figure below shows again the heat transfer coefficients but the ones related to the discharging experiments are calculated by using the same mass flow rate of the charging experiments (average mass flow rate of 0.023 m^3/s). This theoretical mass flow rate is used in order to better compared the charging and discharging experiments. Indeed during the experiments performed it was difficult to set the same mass flow rate because of the type of valves in the system. From the plot below is clearly visible that the overall heat transfer coefficients (blue bars) and the inner heat transfer coefficients (orange bars) have close values for all the experiments, both during discharge and charge of the soil box. The inner heat transfer coefficients have an average value of 454 W/m^2K for

the charging experiments, while 430 W/m^{2}K for the discharging ones. The grey bars instead have a different trend in the two types of experiment, charge and discharge. Indeed, during the charge of the soil the average outer heat transfer coefficient is equal to 276 W/m^{2}K, while for the discharge of the soil the average outer heat transfer coefficient is 205 W/m^{2}K.

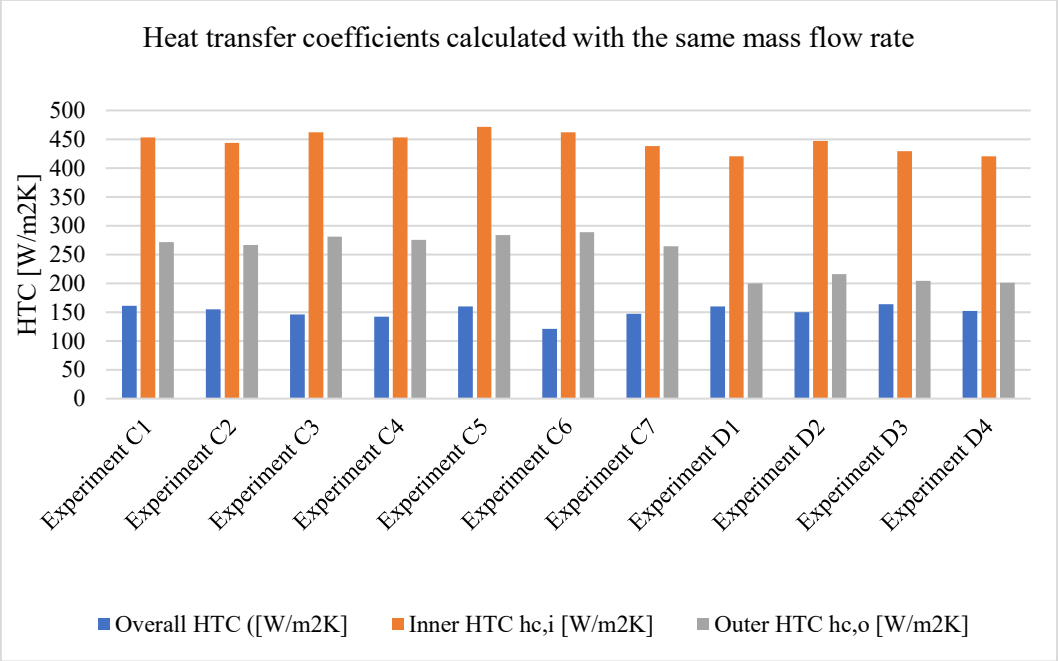

Figure 46: Heat transfer coefficients with the same mass flow rate.

4 Description of the facility at DTU campus

The focus of this chapter is the heat exchange between the fluid in the ground loop and the soil by taking in consideration the fluid properties and by conducting energy balances.
Moreover, the charge of the soil is analysed in order to get information regarding this operating mode.

The experimental test facility is a solar assisted ground source heat pump (SAGSHP) system located at the DTU campus in Lyngby. It is in operation since 2014 and the main components of this system are the storage tank, the solar collectors, the measurements devices (thermocouples and flowmeters), the horizontal ground source heat exchanger and the heat pump.

The tank has 725 litres capacity, and it has 2 concentric sections (tank in tank), one for domestic hot water production (175 litres) and one for space heating demand (550 litres). The inner part of the storage is used for DHW, while the outer one for SH water (Figure 46).
Moreover, in the top part of the tank is stored water with a set point temperature of 50°C for DHW, while in the lower one 35°C for SH water. Stratification is a key factor to fulfil the production of DHW and SH water because it improves the process of energy storing. Multiples sensors are placed inside the tank in tank at different heights.
The tank is used to store the SH water and DHW for a hypothetical single-family house, with an annual SH demand of 2800 kWh and 1825 kWh for DHW. The DHW tapping is set to be the same every day of the year, while for the SH tapping it varies along the year considering the change in the seasons.

The evacuated Kingspan tubular solar collectors have a total gross area of 12.5 m^2 (total aperture area is 9.6 m^2) and they are located on a 12° southwest facing roof with a tilt of 45°.
Solar collectors are connected both to the tank but also to the ground loop heat exchanger. For each of these connections, a plate heat exchanger is placed to divide the circuit of the solar collectors and of the two secondary circuits that go to the tank and to the ground. This is done because of different fluids in each circuit (Figure 46).

The heat generated by the solar collectors is delivered in the outer tank by the use of a inlet stratifier that allows thermal stratification of the water, while colder water is taken from the bottom of the tank, and it is sent to the plate heat exchanger where it is heated up thanks to the heat collected by the solar collectors.

Heat from the heat pump can be sent instead with two different pipes to the tank depending on the temperature of the water produced: one pipe delivers water in the top part of the outer tank, the

other one in the lower part. In this last pipe, the top is closed and there are small holes on the sides of the pipe in order not to release water on the vertical direction. This is done to avoid a mix of the two different temperature layers in the outer tank. Then colder water is taken from other two pipes and sent back to the heat pump where it is heated up by using energy taken from the ground.

Five circulation pumps are used to run the system. In Figure 46, P5 and P6 are related to the condenser and evaporator of the heat pump; P1 circulated the collector fluid in the solar collectors loop, a mixture of propylene glycol (35%) and water (65%); P2 transfer the heat from the solar collectors loop to the storage tank; P3 is used for the charging mode when heat absorbed by the solar collectors is sent to the ground loop and not to the tank.

The fluid in the horizontal ground loop heat exchanger is a mixture of 35% isopropyl alcohol (IPA) and 65% water. In the following pages an analysis is conducted regarding the properties of this fluid in the ground loop.

Figure 46 shows a schematic representation of the system with all the components and different types of sensors placed in specific location.

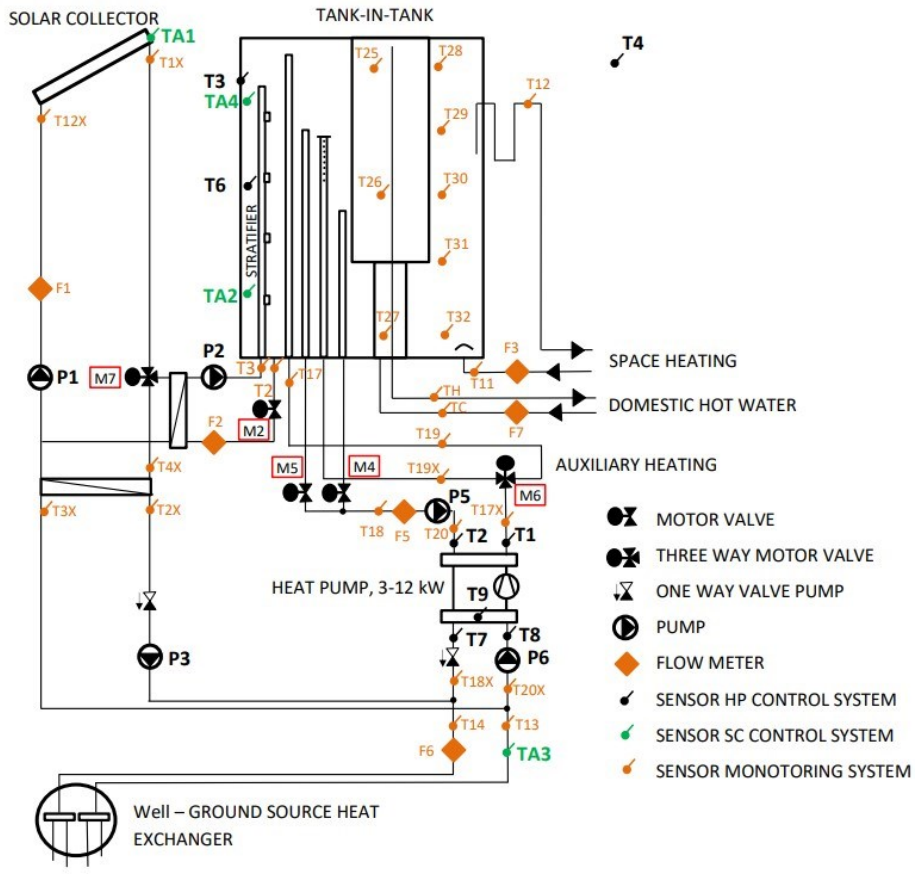

Figure 46 : schematic representation of the test facility.

The heat pump in operation has a power range between 3 and 12 kW thanks to an inverter able to change the frequency between 30 and 70 Hz, thus regulating the compressor of the heat pump.

Figure 47 shows the storage tank, the heat pump and the evacuated tubular solar collectors.

Figure 47: the storage tank (top left), heat pump unit (top right), solar collectors (bottom).

The horizontal ground loop heat exchanger has two loops of 120 m pipes, in total 240 m. The size of the ground loop heat exchanger is 8.5 m wide and 30 m long. The pipes are spaced 1.2 m between each other and buried 1 m below the surface level.

Temperature sensors are placed close to the pipes at 3 different heights (0.5 m, 1 m, 1.5 m under the surface) but also at different depth until 10 metres below the surface to study the temperature variation of the ground along the year.

Figure 48 below shows the arrangement of the sensors and the sizes of the ground loop heat exchanger.

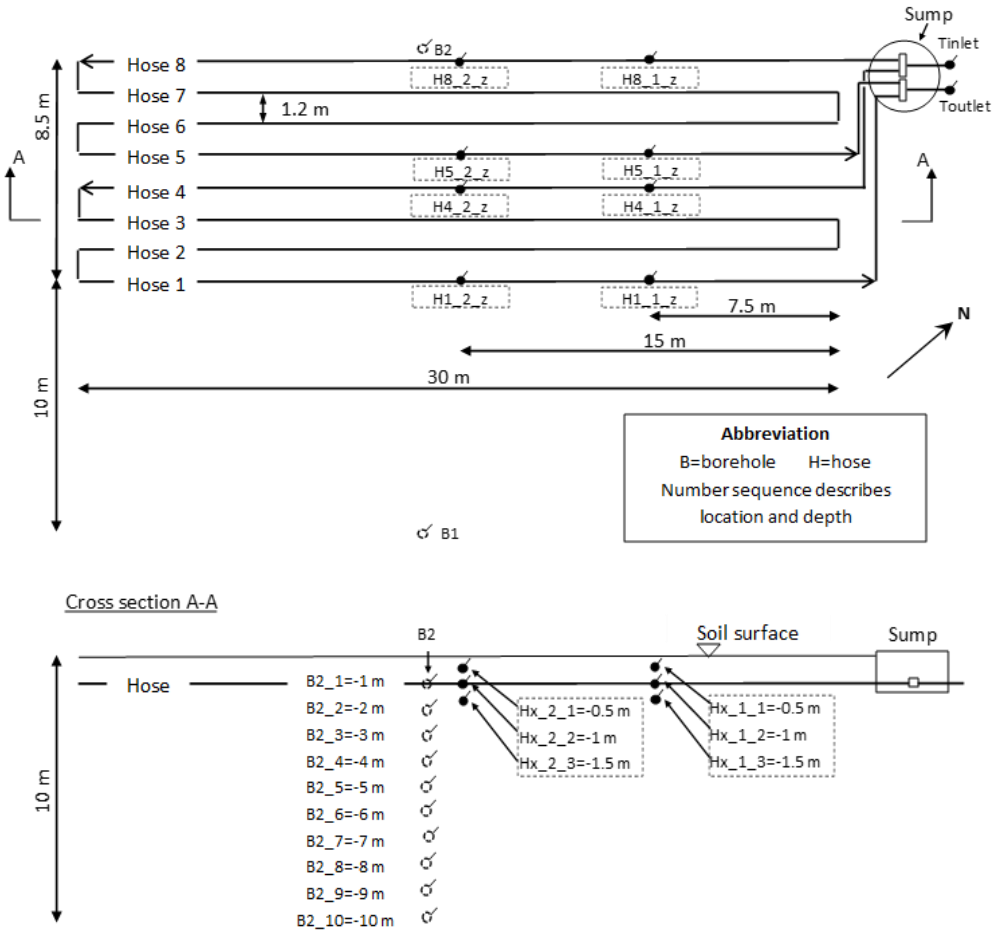

Figure 48: ground loop heat exchanger and location of the sensors

4.1 IPA properties

In the following pages an analysis regarding the properties of the mixture (IPA and water) in the ground loop is carried out with the use of Refprop software. It is also conducted an analysis to verify the heat balance between soil and ground loop during the heat transfer.

In order to perform the energy balance in the correct way, the true values for the properties of the fluid are considered. A sample of fluid is taken from the ground loop and the composition is analysed. The fluid sample is put in a vertical graduated cylinder. Indeed, after several years of operation some leakages or a phenomenon of stratification may have occurred during the long period of not utilisation of the facility due to maintenance. With the use of the vertical graduated cylinder, the fluid is let inside it for several weeks in order to study possible signs of stratification; every 2 weeks few drops of fluid are taken from the top and the bottom of the cylinder and an analysis with a refractometer is done to see if a change in the composition of the fluid occurs. From

all the measurements, no signs of stratification are observed, so the composition of the sample taken from the facility is assumed not to be affected by any stop in the operation or by any leakages.

Figure 49 on the left shows the device, called refractometer, used to check precisely the percentage of IPA inside the water in the ground loop. The refractometer shows on a graduated scale the level of IPA in the water; it is just necessary to put a few drops of the fluid in the inclined glass and look backlit inside the device. A blue line will start to go up and it will stop horizontally on a specific level, which shows the percentage of isopropyl alcohol. Figure 49 on the right shows the scale that is visible by looking inside the device.

Figure 49: refractometer on the left, scale of the refractometer on the right.

With the use of the refractometer, it is verified that the percentage of IPA in the water is around 35%, value used when the ground loop was charged with the water – IPA mixture at the start of the operation in 2014.

Density and specific heat are however function of the temperature at which the fluid in the ground loop operates. Thus, an average value of density and specific heat is considered, with reference to the temperature range at which the fluid operates along year. It is assumed a range between –5°C and +35°C: the lowest value during the cold month, the highest for charging operation mode that can be expected along the warmer months (Table 13).

Temperature [°C]	Density [kg/m^3]	Cp [kJ/kgK]
-5	933.2	3.54
0	932.2	3.52
5	930.7	3.53
10	929.1	3.54
15	927.2	3.55
20	925.1	3.56
25	922.9	3.57
30	920.5	3.58
Average	***927.6***	***3.54***

Table 13: properties of IPA for a 35% concentration, values taken from Refprop.

The above data are used to determine the equations that express density and specific heat as function of the temperature (Figure 50). Specific heat does not vary significantly in the temperature range considered, while the density decreases from 933 kg/m^3 until 921 kg/m^3.

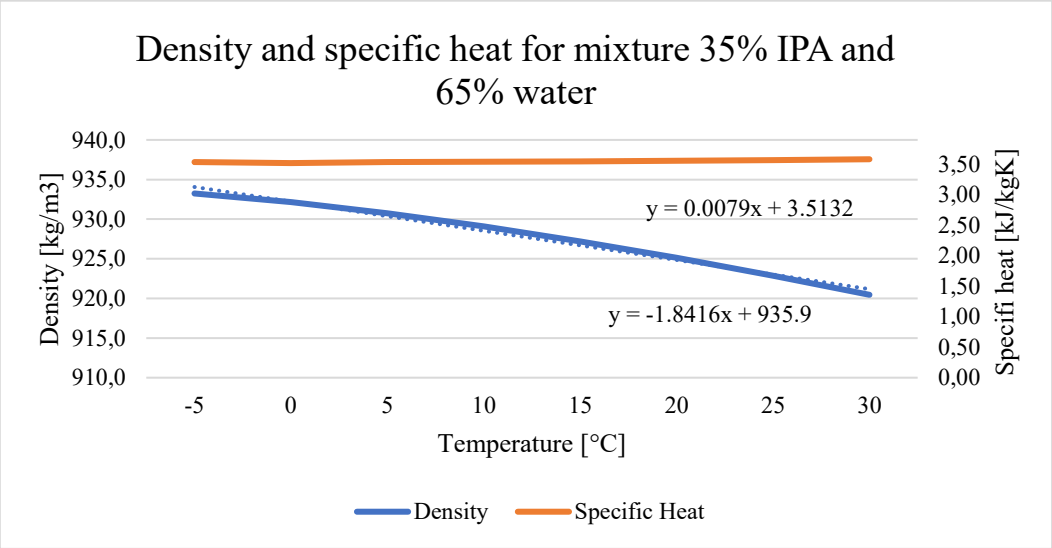

Figure 50: Density and specific heat for the ground loop fluid.

Density [kg/m^3] and specific heat [kJ/kgK] of the mixture as funtion of the temperature are given by:

$$Density = -1.8416 * T14 + 936 \quad (4.\ 1)$$

$$Specific\ heat = 0.0079 * \frac{T13+T14}{2} + 3.513 \quad (4.\ 2)$$

Where T13 and T14 are the outlet and inlet fluid temperatures in the ground loop heat exchanger. Because the fluid changes temperature while it goes through the ground loop, it is assumed to calculate the specific heat considering the average temperature between inlet (T14) and outlet (T13), while for the density just the inlet temperature T14, which is the closest sensor to the flowmeter. Indeed, in order to convert the volumetric flow rate given by the flowmeter into mass flow rate, the density has to be calculate just with the value of temperature T14.

The above equations for the values of density and specific heat are then used for the monthly energy balances explained in the next paragraph.

4.2 Energy balances

Energy balances are carried out to analyse the energy flow in the GSHP system. The period considered for every energy balance is 1 month and the properties of the fluid (density and specific

heat as function of the temperature) shown with equations 4.1 and 4.2 are used for the calculations. The acquisition time of the system is 1 minute and thus all the values calculated each minute are then summed in order to give the monthly energy balance.

Regarding the ground loop and the normal operation of the system (energy from the ground to the tank), the fluid goes from the ground (low temperature heat source in Figure 51) to the heat pump where it releases energy in the evaporator, then it goes back in the ground. Afterwards water absorbs heat from the refrigerant in the condenser of the heat pump, it is heated up and it is sent from the heat pump to the tank (high temperature heat source). In this process the electricity required for the operation is absorbed by the compressor of the heat pump (consumed work).

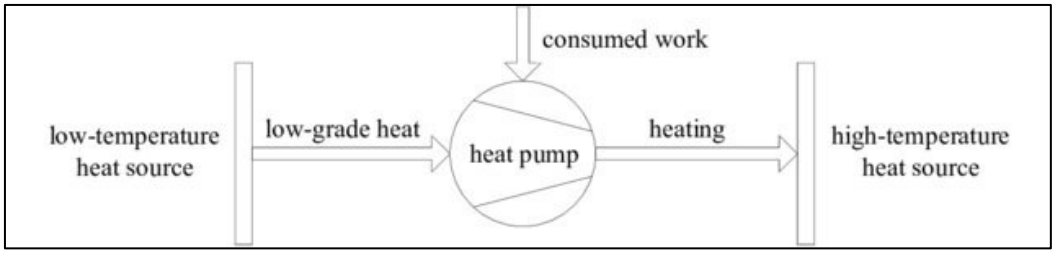

Figure 51: Energy flow during heat pump operation.

In the condenser of the heat pump, the heat absorbed by the water Q_{cM} (heat at the condenser measured) and the heat released by the refrigerant Q_{cC} (heat at the condenser calculated) must be the same. They are function of the following parameters:

$$Q_{c_M} = f\ (T17X; T20)$$

$$Q_{c_C} = f\ (Q_{e_M}; P_{e_M})$$

Where T17X is the outlet temperature of the water from the condenser that goes to the tank, T20 is the inlet temperature of the water coming from the tank in the condenser, Q_{eM} is the heat released by the fluid of the ground loop to the refrigerant in the evaporator of the heat pump and P_{eM} is the energy absorbed by the compressor in the heat pump.

Q_{cM} is calculated taking into account the variation of temperature (T17X – T20 in Figure 46) of the water between the outlet and inlet of the condenser. Q_{cM} [kWh/min] is given by:

$$Q_{c_M} = \frac{m_{F5}}{1000} * \rho_{water} * c_{p_{water}} * (T17X - T20) * \frac{1}{60} * \frac{1}{1000} \qquad (4.\ 3)$$

Where m_{F5} [l/s] is the volumetric flow rate of the water in the auxiliary secondary loop that goes from the heat pump to the tank, ρ_{water} [kg/m^3] is the density of the water, $c_{p,water}$ [J/kgK] is the specific heat of water, T17X is the outlet temperature from the heat pump, T20 is the inlet temperature in the heat pump.

All the values of Q_{cM} calculated for each minute are summed to have the monthly Q_{cM}.

Q_{cC} is instead calculated as sum of Q_{eM} and P_{eM}:

$$Q_{c_C} = P_{e_M} + Q_{e_M} \quad (4.\ 4)$$

Where P_{eM} is the power absorbed by the compressor given by the acquisition system and Q_{eM} is function of T18X and T20X, which are the inlet and outlet temperatures of the fluid (water + IPA) in the ground loop heat exchanger. The difference between T18X and T20X is used to find the heat released by the fluid to the refrigerant in the evaporator of the heat pump.

Equations 4.1 and 4.2 for the properties of the fluid in the ground loop are implemented in Excel for the calculation of Q_{eM} in order to use the correct values of density and specific heat that are function of the temperature. Q_{eM} [kWh/min] is thus given by:

$$Q_{eM} = \frac{m_{F6}}{1000} * (-1.8416 * T14 + 936) * \left(0.0079 * \frac{T13+T14}{2} + 3.513\right) * (T20X - T18X) * \frac{1}{60} * \frac{1}{1000} \quad (4.\ 5)$$

Where m_{F6} [l/s] is the volumetric flow rate of the mixture (water + IPA) in the ground loop, $\rho_{mixture}$ [kg/m^3] is the equation in the first bracket function of the inlet temperature (T14) in the ground loop, $c_{p,mixture}$ [kJ/kgK] is the equation in the second bracket function of the average temperature between inlet (T14) and outlet (T13) in the ground loop, T20X is the inlet temperature in the heat pump, T18X is the outlet temperature from the heat pump.

In order to check the validity of the energy balance, a relative error is calculated:

$$e = \frac{|Q_{c_C} - Q_{c_M}|}{Q_{c_M}} \quad (4.\ 6)$$

Figure 52 shows the errors for each month. The results are all below 6% which is an acceptable value if losses, such as the heat transfer in the plate heat exchangers or the thermal losses in the pipes connections close to the heat pump, are considered.

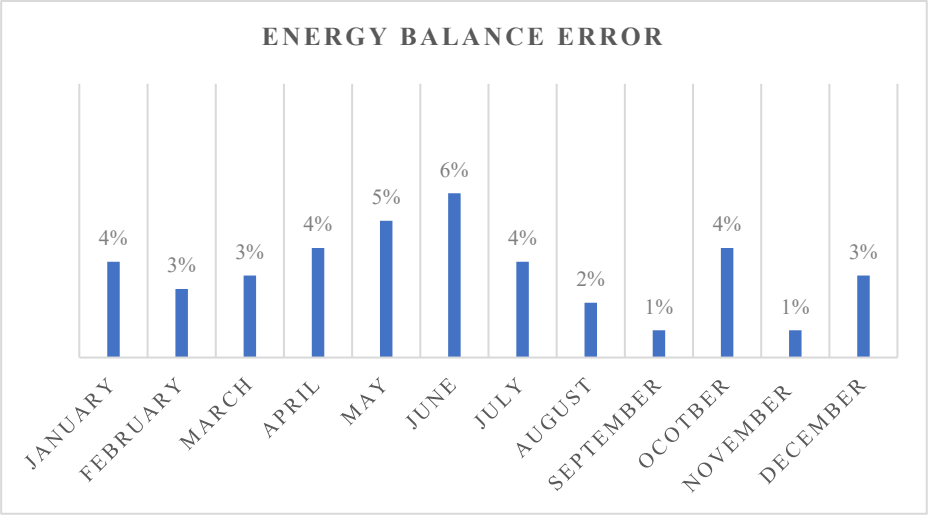

Figure 52: Energy balance error for each month.

4.3 Contribution of solar collectors for the charge of the soil

There are mainly two situations when the charge of the soil occurs. Firstly, when the thermal load is low, for instance in summer periods, and thus the temperature of the storage tank is stable: it is not needed to send energy from the collector to the tank, but instead it can be used for the charge of the soil. Secondly, if the water produced by the solar collectors is not warmer than the minimum temperature required by the storage tank, it can be sent to the ground for the charge of the soil.

A schematic representation of the configuration during the charge of the soil has been already shown in Figure 13. With this operating mode, it is possible to absorb solar energy that otherwise wouldn't be used. Thanks to the secondary loop that connects the main solar collectors loop with the ground loop, energy is sent and stored partially in the ground, but part of it is later dissipated and lost, but still with this operating mode energy savings can be gained by the system; for instance, a greater soil temperature as a result of the soil charge means higher COP of the heat pump when it is in operation, due to a smaller temperature difference between hot and cold sink. Moreover, a lower electricity consumption in the compressor to run the heat pump is required.

Taking into account that the charge of the soil depends on the solar radiation availability, the most relevant months in which the charge of the soil has a considerable influence are now presented. In order to see when this mode is in operation, it is necessary to consider pump P3 (Figure 46) and analyse when it is working. Data collected from the facility in 2019 are used.

Figure 53 shows the energy sent from the solar collectors to the ground considering 4 months. It is clear the difference between April (397 kWh) and August (328 kWh) regarding the energy from the

solar collectors to the ground compared to December (10 kWh) and February (19 kWh). The charge of the soil in the winter months rarely occurs because of the high thermal load that requires heat to be sent from the ground to the storage tank (heat pump operation) and from the collectors to the tank, when solar collectors can produce hot water of minimum 35 °C.

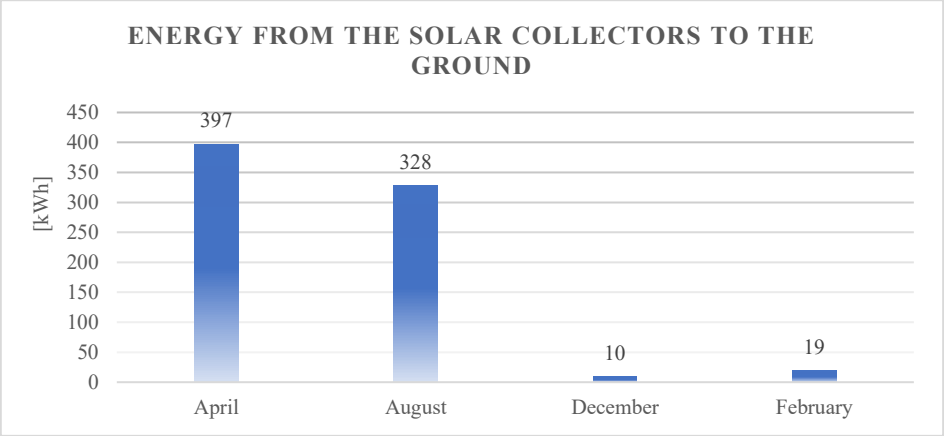

Figure 53: Energy from the collectors to the soil during the charge operating mode.

Figure 54 shows 3 different curves regarding the charge of the soil, the heat pump operation and the average daily global horizontal irradiation (*GHI*). The yellow curve (solar irradiation in the secondary axis) increases from January until June, the month of the year with the longest days and highest amount of radiation, and then it decreases after the summer months. The red curve (charge of the soil) has a similar trend that follows the yellow line: the monthly hours when the pump P3 works in order to charge the soil increases significantly, having the highest values from April until August. Regarding the data from 2019 used in this analysis, the maximum hours for the charge of the soil are in July (299 hours). Lastly, the green curve shows the hours of operation of the heat pump when pump P6 (Figure 46) works. In this case, energy is taken from the ground and it is sent to the facility. It has an opposite trend compared to the charge of the soil, with the highest values of 295 and 293 hours in the winter months (January and December).

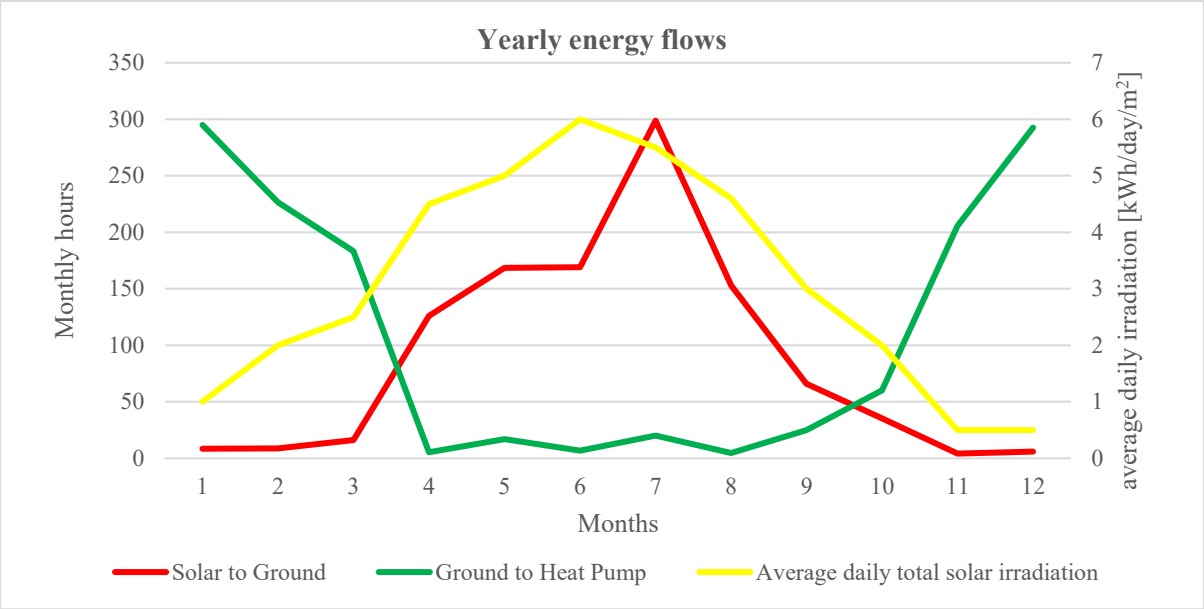

Figure 54: Yearly energy flow regarding the charge of the soil, the heat pump operation and the solar radiation.

In July, the hours for the charge of the soil are high because the storage tank temperatures in the facility stay for long periods during the month above the set point values of 35°C for SH water (green dot line in Figure 55) and 50 °C for DHW (blue dot line). This is due to a low thermal load compared to other months and thus the energy absorbed from the collectors can be sent to the ground and not to the tank. Figure 55 shows the temperature profiles of sensors T25 (DHW, sensor in the top of the inner tank in Figure 46) and T30 (SH water, sensor in the middle of the outer tank in Figure 46).

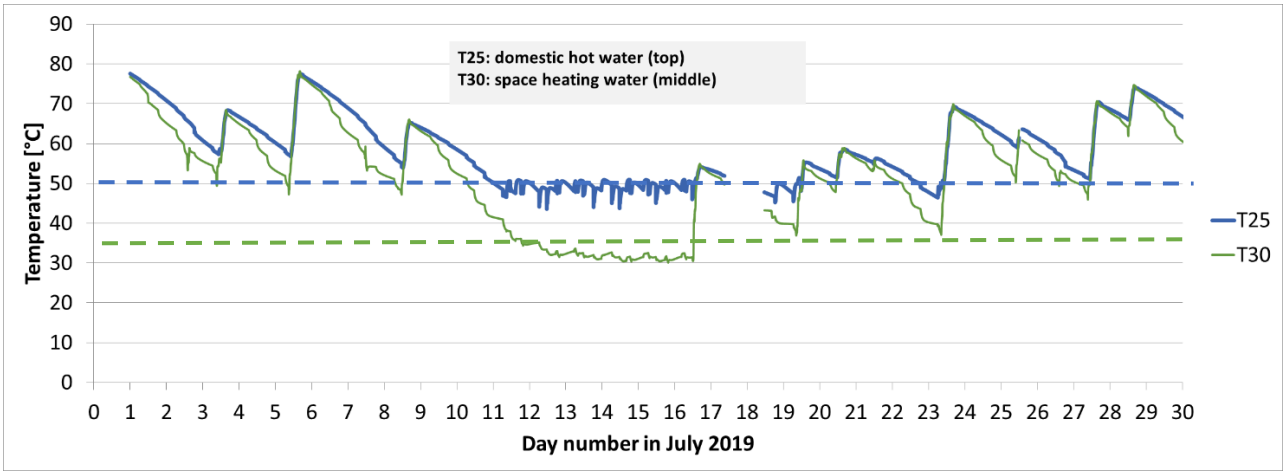

Figure 55: Temperatures profiles of the sensors for DHW (T25) and SH water (T30).

It is also interesting to analyse the temperature range at which the charge of the soil occurs. Figure 56 shows the T14 temperature profile (blue curve, inlet temperature in the ground loop) for the 1st and 20th of July, the month with the highest monthly hours of soil charge as previously shown.

Moreover, the green curve shows when pump P3 is in operation and sends heat from the solar collector loop to the ground. The value of T14 (dot red lines) at which pump P3 starts working is the initial temperature for the charge of the soil. In the control system of the facility this initial temperature is set to 21 °C, also visible from the plots below. It means that the solar collectors will start to charge the soil and P3 to operate when the hot water produced will be at least 21 °C.

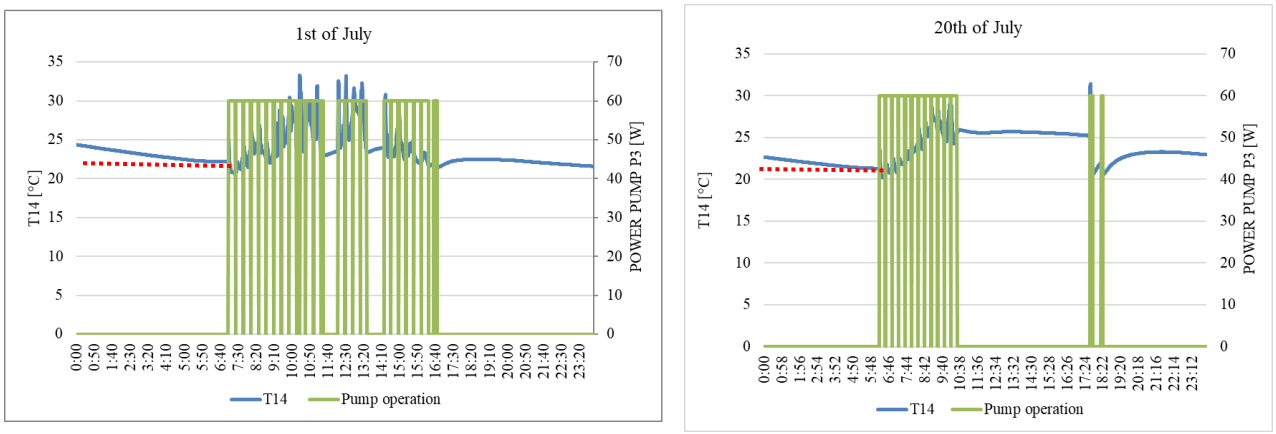

Figure 56: T14 (inlet temperature in the ground loop) and pump P3 operation for the 1st and 20th July.

The green curve shows a frequent oscillation because the control system of the facility stop the charging operating mode every 20 minutes to evaluate the temperature in the collectors. If it is warm enough, the charging operating mode can be stop and energy can be sent from the collectors to the tank.

5 Simulation on TRNSYS

This chapter presents a model of the GSHE that has been designed on Transient System Simulation Tool (TRNSYS). The aim of the simulation is to calculate with different operating conditions along the year the temperature difference between the inlet and outlet in the GSHE considering the measured and calculated values, in order to validate the model. The inlet temperature in the GSHE is called T14M, the calculated outlet temperature T13C and the measured outlet temperature T13M. Simulations are focused on short periods of the year in which there is only one of the 2 operating modes considered, charge or discharge of the soil. The results shown in Table 12 and Table 13, the PSCR and the IPA properties, are implemented in the model in order to have reliable outcomes. Data from 2019 are used as inputs for the calculations.

5.1 Ground source heat exchanger TRNSYS model

The ground source heat exchanger TRNSYS model is designed by considering the configuration of the ground loop in the facility shown in Figure 48.

Figure 57 shows the TRNSYS model with the main components and connections needed. The block *"System Measurements"* on the top contains input data collected in 2019: temperatures of the soil, temperatures of the water and flow rates in the ground loop, energy absorbed by the pumps. These data are used by the model as starting conditions for the calculation of T13C (value calculated by the model) for the period considered. Ambient temperature, flow rates and soil temperature data are sent from this block to the *"pipe"* blocks and to the *"GSHE"* block (black dotted lines in Figure 57).

The block called "*Equations"* contains the equations needed to read correctly the values of temperatures from the *"System Measurements"* block to be sent to the pipes and to read the values of flow rate that the pipes require for the calculations. The block "*Flow pipe in"* represents the starting pipe located inside the facility and the inputs of this component are the inlet flow rate and the inlet initial temperature from the *"Equations"* block, and the indoor temperature of the facility coming from the block *"System Measurements". "Flow pipe out"* is the next block which represents the outdoor pipe that leads to the manifold, and it is exposed to the ambient temperature (value given from the *"System Measurements"* block). The outputs of the "*Flow pipe in"* block are the input for this one, as in all the subsequent components. Afterwards, the *"Flow diverter"* block, which represents the manifolds in the real facility, divides the flow rate in 2 streams before it goes in the *"GSHE"* block. This block is a horizontal ground heat exchanger in which pipes are set to be

spaced 1.2 m between each other and 1 m below the surface, following the configuration in Figure 48; properties, sizes of the pipes and direction of the flow are chosen based on the real facility. A specific fluid circulates through the GSHE and its properties (values of density, specific heat, viscosity and thermal conductivity) can be set in the *"GSHE"* block, taking into account the results obtain in chapter 4, regarding the IPA properties. Also the soil properties and the PSCR are implemented in this block, considering the results obtained from the experiments in chapter 3. More information regarding the boundary conditions and the soil model (node size and mesh parameters) can be found in [22].

To complete the scheme after the *"GSHE"* block, the fluid goes to the *"Flow diverter-2"*, where the flow rates of the 2 ground loops are joined, then to the *"Return pipe out"* and lastly to the *"Return pipe in"*.

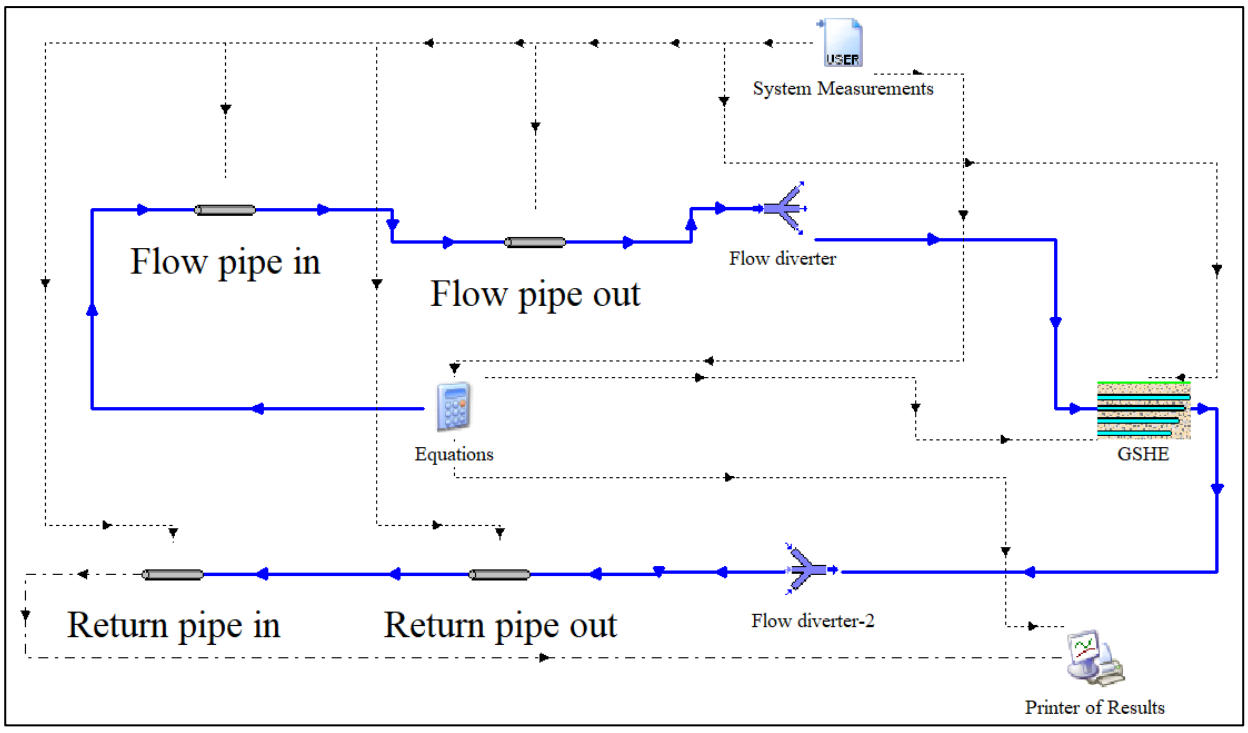

Figure 57: GSHE TRNSYS model.

The output of interest from the *"Return pipe in"* block is the calculated outlet temperature T13C. This value is sent for each iteration of the simulation to the *"Printer of Results"* block. This block plots the value of T13C, T13M, T14M, the flow rate called F6 of the flowmeter, when the heat pump is in operation during the discharge of the soil, or the flow rate called F3 of the flowmeter during the charge of the soil. In the real facility, there is just one flowmeter called F6, as shown in Figure 46: depending on which pump is in operation, pump P3 (charge) or P6 (discharge), the flow rate is called F3 or F6 by the *"equation"* block in the model. T13M, T14M, F3 and F6 values come from the *"Equation"* block and previously from the *"System Measurements"* block. The *"Printer*

of Results" block generate also an *"Output"* file with all the calculated values of T13C and measured (T13M, T14M, F3 and F6) with a timestep of 1 minute. These data are then used in Excel to calculate the temperature difference between the inlet and outlet in the GSHE with the measured and calculated values and results are compared.

5.2 TRNSYS simulations and results

Due to the fact that the *"GSHE"* block can only read constant values as inputs and not functions, the model does not allow to consider the PSCR and the properties of the fluid (density and specific heat) as function of the temperature. Indeed in chapter 3 and 4 it is investigated how these parameters depends on the temperature level of the fluid and on the operating mode that occurs. In the simulations performed, constant values are used for the density and the specific heat of the fluid in the GSHE (values taken from Table 13) and for the PSCR (average values from Table 12). Constant values implemented in the model for each simulation are chosen based on the type of operating mode that occurs in the period considered, charge or discharge of the soil.

Because the temperature dependence of the parameters can't be considered in the model, the simulation must be performed in short periods in which just one type of operating mode occurs. As shown in Figure 54, in some months during the year one operating mode is dominant. In January the hours of operation of the heat pump are really high, while for the charge of the soil the number is negligible; in July is the opposite, with a remarkable number of hours for the charge and a negligible number for the discharge of the soil. For this reason, the simulations performed are referred to these periods when only one type of operating mode occurs. The simulation time is equal to 1 day in January and 1 day in July: short periods in order to have surely only one type of operating mode, because the model uses constant values for the parameters considered.

Regarding the *"GSHE"* block, it is assumed one type of soil for the analysis with constant properties (density of the soil layer, specific heat and thermal conductivity). This block requires also to set some other parameters for the heat transfer between soil and GSHE: soil temperatures and fluid temperatures are necessary for the calculations in each timestep.
Start temperature profiles are considered based on the Kusuda equation [27], which is implemented in the *"GSHE"* block for the calculation of the soil temperatures during the simulations. It allows to calculate the temperature of the soil as function of the depth (z) and the day of the year. It is given by:

$$T_{BC}|_{z,day} = T_{ave} - T_{amp} * exp\left(-z * \left(\frac{\Pi}{365*\alpha_{soil}}\right)^{0.5}\right) * cos\left(\frac{2*\Pi}{365} * \left(Day - Day_{min} - \frac{z}{2} * \left(\frac{365}{\Pi*\alpha_{soil}}\right)^{0.5}\right)\right) \quad (5.\ 1)$$

Where T_{ave} is the average deep earth temperature [°C], T_{amp} is the amplitude of variation [°C], z is the depth [m], Day_{min} is the day of the year with the minimum surface temperature, α_{soil} is the thermal diffusivity of the soil [m^2/s], function of the thermal conductivity k [W/mK], density ρ [kg/m3] and specific heat c_p [J/kgK]. All these parameters for the Kusuda equation have to be set in the *"GSHE"* block at the begin of each simulation and the values are chosen by comparing the measured soil temperature profiles of borehole B2 (Figure 48) with the temperature profile that Kusuda equation calculates. The parameters that give the best fit between the 2 curves (measured temperature profile and Kusuda temperature profile) are chosen and implemented in TRNSYS for both the simulations.

5.2.1 Simulation of the TRNSYS model for the 1st of January

Parameters implemented in the *"GSHE"* block in this first simulation in order to give the best fit between the measured temperature data of borehole B2 (dot curve) for the 1st of January and the Kusuda temperature profile (continue curve) are shown in Figure 58. An iteration was carried out until the best suitable fit was found.

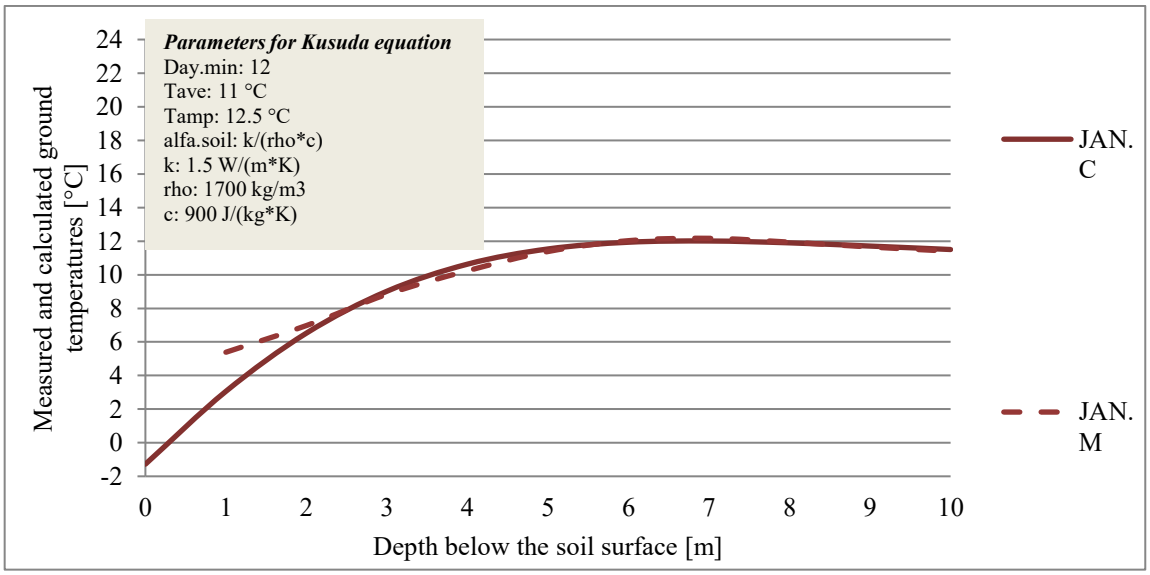

Figure 58: Soil temperature profiles, measured and calculated curves for the 1st of January.

After setting all the values required by the model (simulation time, fluid properties, soil properties and Kusuda parameters for the soil temperature profile) the simulation was performed.

Figure 59 shows the results for the 1st of January, when it is assumed only the discharging operating mode, meaning that T14M is supposed to be lower than T13M and T13C because heat is absorbed

by the fluid from the soil in the ground loop. Constant values implemented for this simulation of discharge are: $PSCR_{D,average}$ = 0.013 m^2K/W, fluid density $\rho_{average}$ = 927.6 kg/m^3, fluid specific heat $c_{p,average}$ = 3.54 kJ/kgK. The red curve represents T13C [°C], the blue one T13M [°C], the purple one T14M [°C] and the green one F6 [kg/h]. The orange line (F3) is equal to zero for all day, meaning that for the 1st of January there is no charge of the soil. It is clearly visible that T13C and T13M have similar trends when the heat pump is in operation, meaning F6 ≠ 0 kg/h. This shows that, starting from the value of T14M, the model is able to calculate a value of T13C at the outlet of the GSHE really close to the measured value T13M.

Figure 59: TRNSYS simulation for the 1st of January. Values of T13C (red curve), T13M (blue curve), T14M (purple curve), F6 (green curve) are plotted. Temperature in [°C] and flow rate in [kg/h].

It is interesting to analyse the variation of the temperature difference between the inlet and outlet of the GSHE considering the measured values (T14M, T13M) and the calculated value (T13C). Figure 60 reports this temperature difference, showing a similar trend for the red curve (T13C – T14M) and blue curve (T13M – T14M). The y axe represents the temperature difference in [K], the x axe shows the minutes of the day (1st of January) in which the heat pump is in operation (discharge of the soil), meaning that flowrate F6 is different from zero. Some values in the graph are negative both for the measured and calculated curve, due to the heat pump stops in the operation for some periods. Indeed, when the heat pump is not in operation (green line equal to 0 kg/h), T13M (blue line) and T14M (purple line) increase because no heat exchange occurs with the ground. Thus at the next heat pump start in the operation (green line not equal to 0 kg/h), for some minutes T14M is always higher than T13C and sometimes also higher than T13M, leading to negative temperature differences. The reasons why in the graph below there are these negative temperature differences

are the following. Firstly, some minutes are required before the fluid, which was stationary during the stop in the heat pump operation, goes from the location of sensor T14M to the outlet sensor T13M. This sensor is supposed to measured the temperature value T13M of the fluid when the heat pump is in operation, meaning that the fluid is circulating and not stagnant in the pipes of the GSHE. Indeed, when the fluid is not circulating, its temperature varies and thus at the new start in the heat pump operation, sensor T13M will measure an incorrect value. Secondly, another reason that justify why in the graph negative values are plotted, is the time of response of sensor T13M and the way it is mounted. Indeed, when the heat pump operation starts, sensor T13 requires some minutes in order to measure the true value of the fluid temperature. For these two reasons negative values are also plotted.

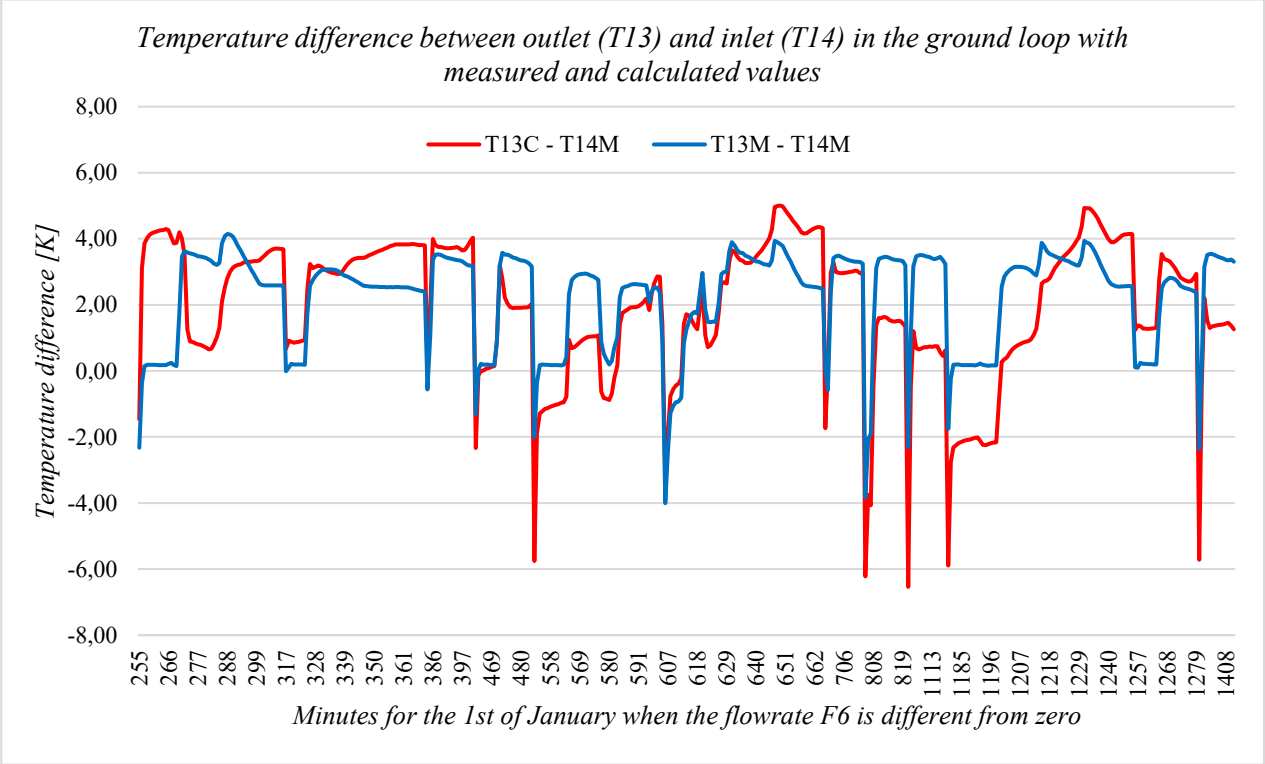

Figure 60: Temperature difference between outlet (T13) and inlet (T14) for the 1st of January in the ground loop.

It is interesting to compare the results by calculating the average temperature difference ($\Delta T_{average}$) for the 2 curves in Figure 60. All negative values are excluded from the calculation because they don't represent correctly the heat pump operation for the reasons previously discussed. It is obtained from the calculations an average temperature difference between T13C and T14M equal to $\Delta T_{average,calculated} = 2.62$ K, while considering T13M and T14M equal to $\Delta T_{average,measured} = 2.46$ K.

5.2.2 Simulation of the TRNSYS model for the 1st of July

Parameters implemented in the *"GSHE"* block in this second simulation in order to give the best fit between the measured temperature data of borehole B2 (dot curve) for the 1st of July and the Kusuda temperature profile (continue curve) are shown in Figure 61. An iteration was carried out until the best suitable fit was found.

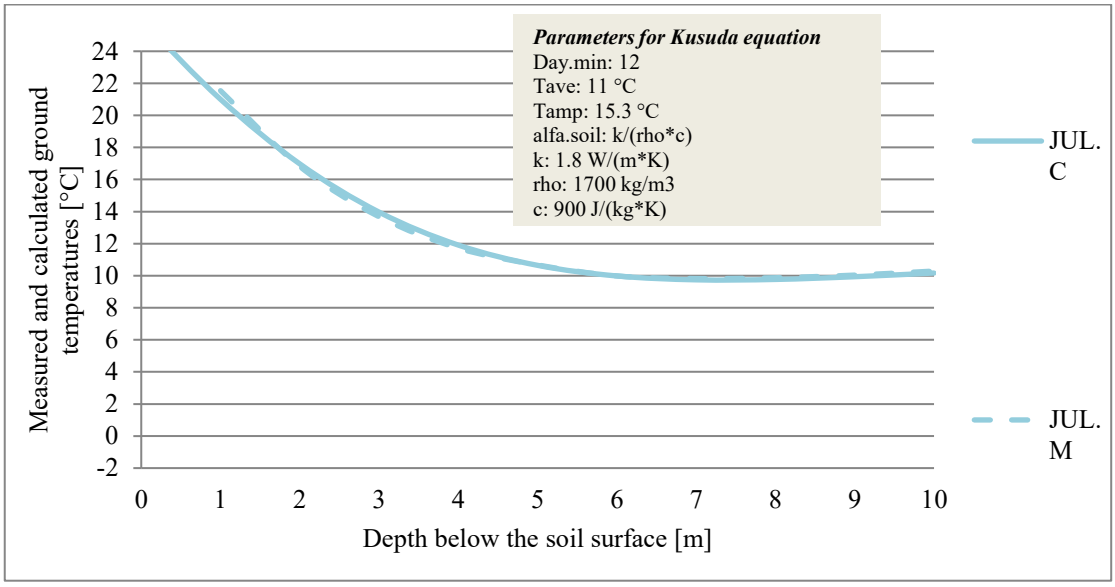

Figure 61: Soil temperature profiles, measured and calculated curves for the 1st of July.

After setting all the values required by the model (simulation time, fluid properties, soil properties and Kusuda parameters for the soil temperature profile) the simulation was performed.

Figure 62 shows the results for the 1st of July, when only the charging operating mode occurs. Constant values implemented for this simulation of charge are: $PSCR_{C,average}$ = 0.007 m^2K/W, fluid density $\rho_{average}$ = 927.6 kg/m^3, fluid specific heat $c_{p,average}$ = 3.54 kJ/kgK. The red curve represents T13C [°C], the blue one T13M [°C], the purple one T14M [°C] and the orange one F3 [kg/h]. The green line (F6) is equal to zero for all day, meaning that for the 1st of July there is no discharge of the soil. It is clearly visible that T13C and T13M have similar trends when solar collectors send heat to the ground (F3 ≠ 0 kg/h). This means that also in this simulation, starting from the value of T14M, the model can calculate a value of T13C at the outlet of the GSHE really close to the real value measured T13M.

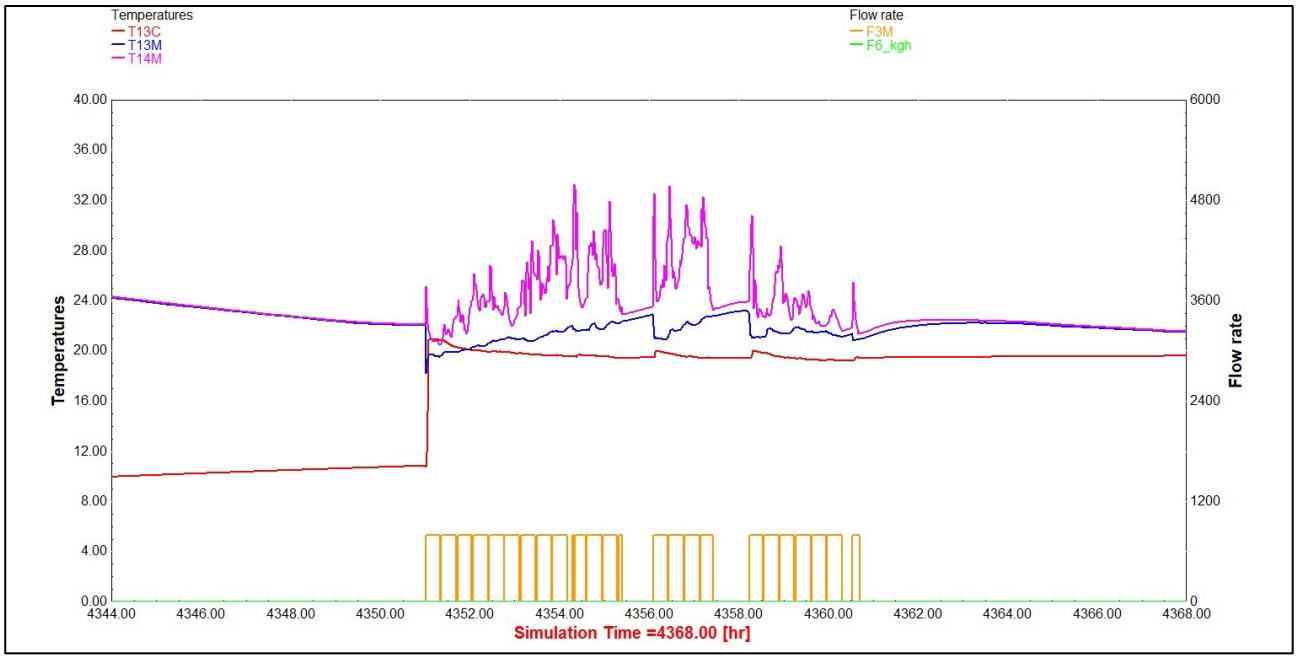

Figure 62:TRNSYS simulation for the 1st of July. Values of T13C (red curve), T13M (blue curve), T14M (purple curve) and F3 (orange curve) are plotted. Temperature in [°C] and flow rate in [kg/h].

Also in this case, it is interesting to analyse the variation of the temperature difference between the inlet and outlet of the GSHE considering the measured values (T14M, T13M) and calculated value (T13C). Figure 63 reports this temperature difference, showing a similar trend for the red curve (T14M – T13C) and blue curve (T14M – T13M). The y axe represents the temperature difference in [K], the x axe shows the minutes of the day (1st of July) during which pump P3 is in operation (charge of the soil), meaning that flowrate F3 is different from zero.

The measured temperature difference (blue line) is always positive, while the calculated temperature difference (red line) is negative just for a small number of minutes precisely when the charge of the soil starts. Indeed, when F3 is not zero anymore around *Simulation time = 4351 hr* in the figure above, there is a small period in which T13C > T14M, meaning that T14M – T13C < 0 as visible in Figure 63.

Moreover the two curves in the plot are straight in some parts because during those periods the charge of the soil does not occur, meaning that F3 = 0 kg/h and no temperature difference is calculated. Thus the points between two different periods of charging are easily connected with a line in Excel.

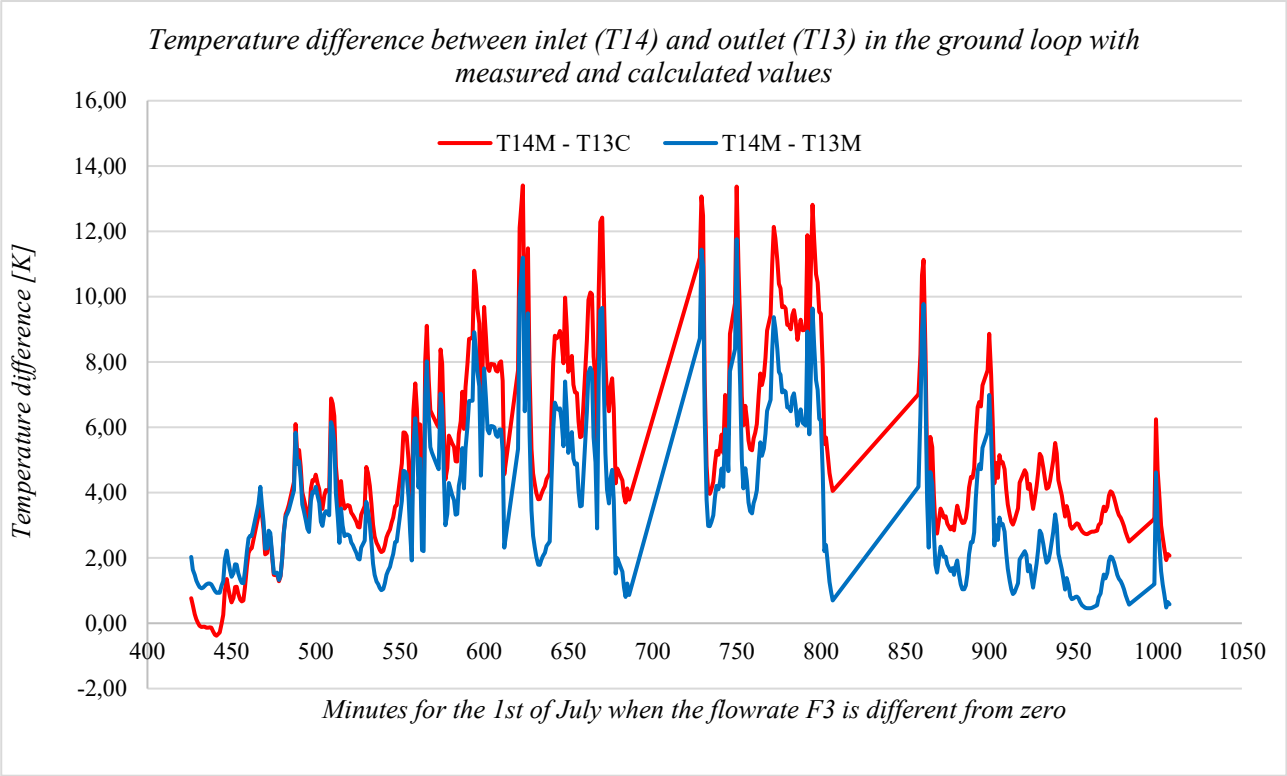

Figure 63: Temperature difference between inlet (T14) and outlet (T13) for the 1st of July in the ground loop.

It is interesting to compare the results by calculating the average temperature difference ($\Delta T_{average}$) for the 2 curves in Figure 63. The negative values (red values around minute 450 in the graph above) are excluded from the calculation because they don't represent correctly the charging mode.

It is obtained from the calculations an average temperature difference between the values T14M and T13C equal to $\Delta T_{average,calculated}$ = 4.54 K, while considering T14M and T13M equal to $\Delta T_{average,measured}$ = 3.67 K.

5.3 Discussion of the results

In the simulations performed only one type of operating conditions is considered for short periods. The average temperature difference between inlet (T14M) and outlet is similar both with the measured (T13M) and calculated value (T13C), meaning that the model gives accurate results with the input data and parameters assumed. $\Delta T_{average}$ between the measured and calculated values differs for less than 1°C for both simulations.

The limitation of this model is due to the fact that long periods can't be simulated because mix operating modes (charge and discharge) are not recognized by the model and thus parameters that depends on the temperature range at which the system operates and on the type of operation can't be varied, but they must be assumed constant, as in the simulations performed. In order run the

simulations for long periods along the year with different operating modes, the TRNSYS model should be improved by taking in consideration the results obtained from the small scale experiment in chapter 3, with reference to the PSCR as function of the temperature level at which the GSHE is in operation, and the results from chapter 4 regarding the temperature dependence of the IPA properties. In particular, the *"GSHE"* block should receive as inputs values of PSCR, fluid density and fluid specific heat that are function of the operating mode and of the temperature level at which the system operates. With this modification, the model would be able to use the correct value for each parameter during long periods of simulation.

6 Conclusions

In this thesis the heat transfer between soil and ground loop heat exchanger and the typical operation conditions of a GSHP combined with solar collectors in different periods of the year are investigated.

Small scale experiments with the soil sample give important information regarding parameters that affect the heat exchange between soil and pipe with 2 operating conditions (charge – discharge) and different temperature ranges. In particular the results show a more favourable heat transfer during the charge of the soil. The HECR varies between 5.3 W/K and 6.3 W/K in the charging operating mode, while between 3.4 W/K and 4.3 W/K in the discharging operating mode. Regarding the overall heat transfer coefficient, it varies between 121 W/m^2K and 161 W/m^2K in the charging operating mode, while between 57 W/m^2K and 99 W/m^2K in the discharging operating mode. Also the PSCR changes with the operating mode considered: in the charging operating mode $PSCR_{C,average} = 0.007$ m^2K/W, indeed the heat transfer better occurs in this case because of the small resistance between soil and pipe, while in the discharging operating mode $PSCR_{D,average} = 0.013$ m^2K/W. Moreover, thermal expansion of the pipe clearly affects the contact with the soil, leading to an higher outer heat transfer coefficient in the charging operating mode. Further experimental investigations with the soil sample could add more knowledge regarding different operating conditions in which the heat transfer could occur.

Regarding the facility considered, the properties of the fluid used in the ground loop and the 2 operating modes are studied. Results show that the density and the specific heat of the mixture water – IPA depends on the temperature level of operation and equations to describe the variation of these parameters as function of the temperature are obtained. Moreover, the operating modes of the facility are investigated and a comparison is made between the charge of the soil and the normal heat pump operation (discharge of the soil), by considering the monthly hours and the energy flows, in order to find the typical operating conditions for different months. July has the highest number of monthly hours (299 h) regarding the charging operating mode, while January the highest number of monthly hours (295 h) regarding the discharging operating mode.

Lastly, a TRNSYS model is designed to simulate the ground loop heat exchanger. Results from the small scale experiments in chapter 3 and from the analysis of the facility operating modes from chapter 4 are taken into account in order to implement the correct parameters in the model. Constant parameters are used and simulations are performed for short periods. The 1st of January, when only discharge of the soil occurs, and the 1st of July, when only charge of the soil occurs, are chosen as simulation periods. The calculated average temperature difference between inlet (T14M) and outlet

is similar both with the measured outlet temperature (T13M) and the calculated outlet temperature (T13C), meaning that the model gives accurate results with the input data and parameters assumed. $\Delta T_{average}$ between the measured and calculated values differs for less than 1°C for the simulations performed.

An improvement of the model is required in order to perform simulations for longer periods; the dependence on the temperature level and on the type of operation mode should be taken into consideration. Equations and results regarding the PSCR, the density and specific heat of the fluid could lead to better results for long simulation periods if correctly implemented in the TRNSYS model.

Bibliography

[1] E. C. G. George Halkos, “Where do we stand on the 17 Sustainable Development Goals? An overview on progress,” *Science Direct,* 2021.

[2] “Internation Energy Agency,” 2019. [Online]. Available: https://www.iea.org/fuels-and-technologies/electricity.

[3] “Internation Energy Agency,” 2019. [Online]. Available: https://www.iea.org/data-and-statistics/data-browser?country=WORLD&fuel=Energy%20supply&indicator=RenewGenBySource.

[4] “Eurostat Statistics Explained,” 2019. [Online]. Available: https://ec.europa.eu/eurostat/statistics-explained/index.php?title=File:Final_energy_consumption_in_the_residential_sector_by_use,_EU,_2019_F2.png.

[5] I. S. Lukas Skalik, “Long term Global Radiation Measurements in Denmark and Sweden,” 2019.

[6] “International Energy Agency,” 2021. [Online]. Available: https://www.iea.org/reports/heat-pumps.

[7] N. J. Kurmayer, “Euractiv,” 17 May 2022. [Online]. Available: https://www.euractiv.com/section/energy-environment/news/netherlands-to-ban-fossil-heating-by-2026-make-heat-pumps-mandatory/.

[8] “Internation Energy Agency,” Internation Energy Agency, [Online]. Available: https://www.iea.org/data-and-statistics/data-browser?country=NETHLAND&fuel=Electricity%20and%20heat&indicator=HeatGenByFuel.

[9] I. E. Agency, “Renewables 2019, Analysis and forecast to 2024,” 2019.

[10] J. Cantor, “John Cantor Heat Pumps,” [Online]. Available: https://heatpumps.co.uk/heat-pump-information-without-the-hype/what-is-the-cop/.

[11] L. X. C. B. B. C. S. P. J. W. Xinru Wang, “A systematic review of recent air source heat pump (ASHP) systems assisted by solar, photovoltaicand and photovoltaic/thermal sources.,” *Science DIrect,* 2019.

[12] C. Wemhoener, “Economical heating and cooling systems for low energy houses,” in *Technology Collaboration Programme on Heat Pumping Technologies*, IEA, 2011.

[13] S. H. Jörn Ruschenburg, “A COMPARATIVE ANALYSIS OF MARKET AVAILABLE SOLAR THERMAL HEAT PUMP SYSTEMS,” Freiburg, Germany.

[14] E. G. E. Council, “EGEC Geothermal Market Report,” 2021.

[15] J. Sipma, “Heat pump – Groundwater to water,” Energy.nl, [Online]. Available: https://energy.nl/data/heat-pump-groundwater-to-water/.

[16] E. Saver, “Energy Saver,” [Online]. Available: https://www.energy.gov/energysaver/geothermal-heat-pumps?msclkid=de407a0ec6f211eca8237427492954df.

[17] X. L. L. D. Cang Tong, “Sensitivity analysis of the ground-coupled heat pump system with horizontal ground heat exchangers in the cold regions of China,” 2019.

[18] Z. C. Yongbao Chen, “Dynamic modeling of solar-assisted ground source heat pump using

Modelica," *Science Direct,* 2021.

[19] J. F. S. F. Junpeng Huang, "Demonstration and optimization of a solar district heating system with ground source heat pumps," *Science Direct,* 2020.

[20] J. K. C. S. P. Byun Kang, "SIMULATION STUDY ON THE PERFORMANCE OF SOLAR AND GEOTHERMAL HYBRID R22 HEAT PUMP".

[21] Chwieduk, "Solar assisted Heat Pumps".

[22] C. Jurado, "Analysis of solar heating / heat pumps systems," 2020.

[23] A. L. Kara, "Investigations of Solar Heating/Heat Pump Systems," 2021.

[24] A. F. Mills, Heat Transfer, CRC Press, 1992.

[25] F. Hamrouni, "Theoretical and experimental investigations of ground source heat exchangers," 2021.

[26] S. Furbo, "Heat Storage for Solar Heating Systems," 2005.

[27] T. E. S. Specialists., "TESSLibs17, Component Libraries for the TRNSYS Simulation Enviroment.," 2013.

[28] "International Energy Agency," 2021. [Online]. Available: https://www.iea.org/reports/heating.